ACS Catalysis

Review

pubs.acs.org/acscatalysis

Toward Understanding Metal-Catalyzed Ethanol Reforming

Daniela Zanchet,[†] Joao Batista O. Santos,[‡] Sonia Damyanova,[§] Jean Marcel R. Gallo,[∥] and José Maria C. Bueno*[,‡]

[†]Institute of Chemistry, State University of Campinas (UNICAMP), P.O. Box 6154, 13083-970 Campinas, São Paulo, Brazil

[‡]Department of Chemical Engineering, Federal University of São Carlos (UFSCar), P.O. Box 676, 13565-905 São Carlos, São Paulo, Brazil

[§]Institute of Catalysis, Bulgarian Academy of Sciences, 1113 Sofia, Bulgaria

[∥]Department of Chemistry, Federal University of São Carlos (UFSCar), P.O. Box 676, 13565-905 São Carlos, São Paulo, Brazil

ABSTRACT: Steam reforming of ethanol (SRE) is a strategic reaction for H_2 production. However, despite considerable work, several aspects of the mechanism and catalytic system for this reaction are not fully understood. There have been many efforts to improve the understanding of the catalysts' behavior during SRE, using both theoretical studies and experimental investigations based on operando characterization techniques. Even though cobalt and nickel are considered the most promising catalytically active metals for industrial SRE, acquiring further knowledge on the reaction mechanism, metal−support interactions, and catalyst deactivation (due to carbon accumulation, sintering, or metal oxidation) will enable the successful design of new and stable catalysts. In this review, we analyze the reaction pathways for metal-catalyzed SRE and discuss the available experimental and theoretical data to suggest alternatives to address three major issues: (i) the impact of particle size and metal oxidation state in the SRE performance; (ii) the importance of metal surface electronic properties to obtain a balanced and stable catalyst; and (iii) the influence of support on the catalyst selectivity and stability. Clarification of these issues is a key point for understanding the SRE reaction and for the development of new high performance catalysts.

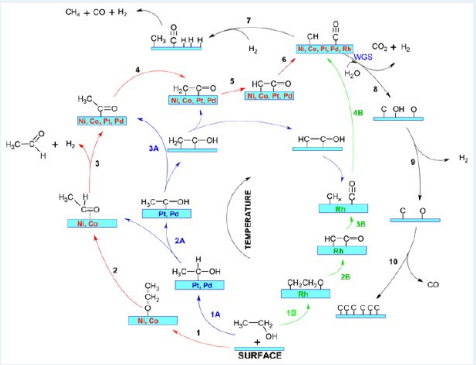

KEYWORDS: *ethanol reforming, hydrogen production, reaction mechanism, metal catalyst, heterogeneous catalysis, biomass conversion, ethanol decomposition*

1. INTRODUCTION

Steam reforming of hydrocarbons, especially methane (SRM), has been widely studied to fulfill the demand for H_2.[1] In industrial processes, steam reforming of natural gas, which consists mainly of methane, is performed using nickel-based catalysts. A thorough understanding of the SRM reaction mechanism and catalyst behavior has been acquired following extensive experimental and theoretical research.[2−4] However, the stability of methane molecule demands the use of high performance catalysts, whose properties may not be suitable for more reactive molecules such as ethanol. For example, the addition of small amounts of Au or Ag to nickel-based catalysts can successfully suppress the growth of carbon filaments in SRM,[5] but this is not effective in the case of steam reforming of ethanol (SRE, eq 1).[6]

The production of H_2 from renewable resources such as ethanol has received a special attention due to the attendant environmental benefits. In SRE, the catalyst must assist the cleavage of C−H, C−C, and O−H bonds, with the fragments recombining to produce CO, CO_2, and H_2. Noble metals would be the best catalyst candidates for SRE due to their greater ability to break C−C bonds,[7,8] and in fact, Rh has been reported to be the most active catalyst for SRE.[9−11] However, the high cost of noble metals has shifted the attention to Ni and Co catalysts, which are also effective in breaking C−C bonds and show high activity in SRE. Their performance, however, suffers from strong deactivation due to the extensive carbon deposition. Karim et al.[12] comparing the catalytic behavior of supported Rh and Co catalysts, concluded that Co was a better option than Rh, taking into consideration CH_4 selectivity and the possibility of regeneration. Because the carbon deposition is a major problem in SRE, the addition of oxygen to the reactant mixture, known as oxyreforming of ethanol (ORE, eq 2), has been used to control the accumulation of carbon. Despite of the lower H_2 yield, the presence of oxygen in ORE has been found to be strategic to avoid carbon deposition[13,14] and to improve the reaction energy balance, relative to SRE.

$$\text{SRE: } CH_3CH_2OH + 3H_2O \leftrightarrows 2CO_2 + 6H_2 \quad (1)$$

$$\text{ORE: } CH_3CH_2OH + (3 - 2x)H_2\text{withO} + xO_2 \leftrightarrows 2CO_2 + (6 - 2x)H_20 < x < 0.5 \quad (2)$$

Received: December 23, 2014
Revised: April 10, 2015
Published: April 15, 2015

DOI: 10.1021/cs5020755
ACS Catal. 2015, 5, 3841−3863

Scheme 1. Representation of the SRE Reaction Pathways as a Function of Temperature for Different Metal Surfaces[a]

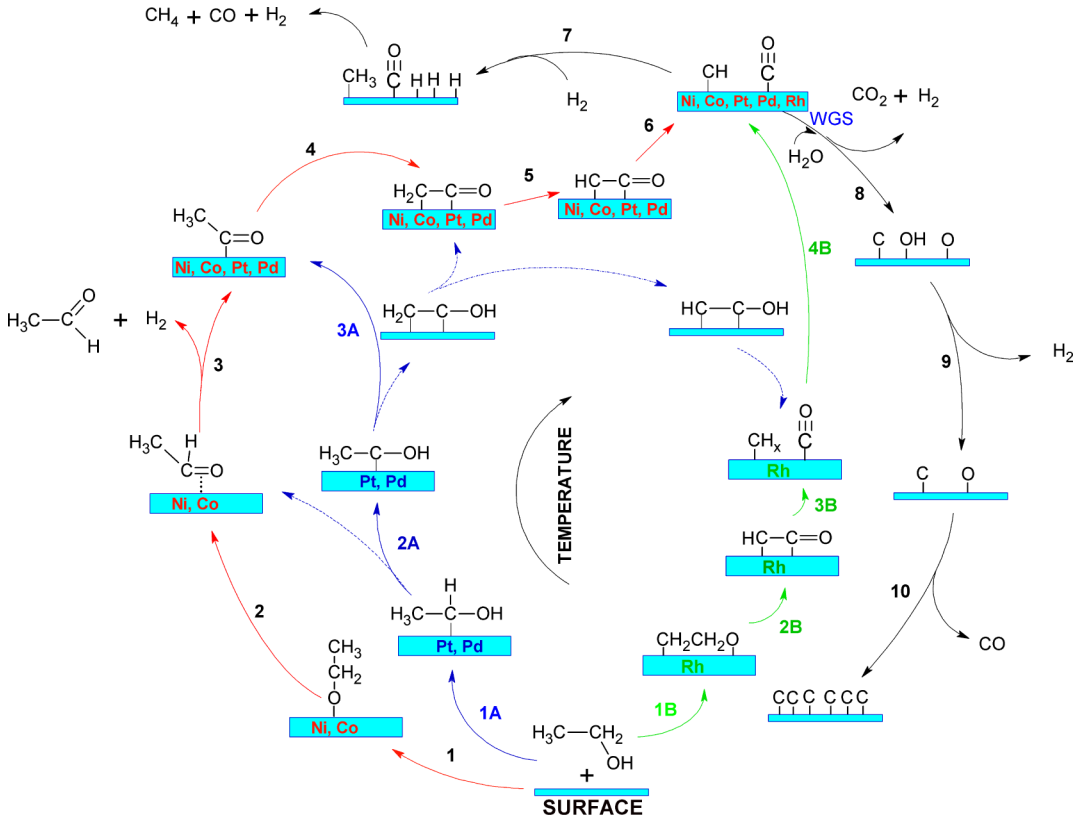

[a]Red, blue, and green colors indicate main routes on Ni or Co, Pt or Pd, and Rh, respectively; dashed lines are secondary routes.

Recent reviews[4,14−18] have described advances in the technology of H_2 production, the development of catalysts for SRE and ORE, the main pathways involved in catalyst deactivation, and aspects of the reaction mechanism. Nonetheless, it is clear that despite the significant efforts, important questions still remain unanswered, so that there is a need for further studies designed for better understanding these reactions.

Based on of theoretical and experimental results, in this review, the reaction pathways and mechanisms of SRE on metals are first analyzed. Then, the three main aspects concerning SRE and ORE are presented: (i) the effect of the metal nature—the impact of the particle size and the metal oxidation state in the SRE performance; (ii) the importance of the metal surface electronic properties to obtain a balanced and stable catalyst; and (iii) the influence of the support on the catalyst selectivity and stability.

We believe that a better understanding of the reaction mechanism and of the three aspects mentioned above should lead toward the development of new high performance catalysts for SRE. In this respect, advances in experimental investigations conducted in situ, or ideally, under operando conditions, as well as theoretical studies, are central aspects to improve the design of SRE and ORE catalysts.

2. REACTION MECHANISMS AND PATHWAYS

SRE involves the activation of ethanol and water on the surface of a metal particle or of a metal oxide support. The effects of the metal oxide support resulting in either a bifunctional or a predominantly monofunctional mechanism are discussed in Section 5. In this section, we discuss the SRE mechanisms when it occurs on a metal surface.

Scheme 1 summarizes plausible reaction pathways involved in the SRE over the metal surface, based on both experimental and theoretical results. The ethanol activation proceeds via three main pathways: (i) by cleavage of OH bond and successive dehydrogenation forming a sequence of intermediates including acetaldehyde (CH_3CHO^*), acetyl (CH_3C^*O), ketene ($^*CH_2C^*O$), and ketenyl ($^*CHC^*O$), represented by steps 1−5 in Scheme 1; (ii) by CH bond activation followed by successive dehydrogenation, preserving O−H bond with formation of intermediates $^*CH_yCH_x{}^*OH$ through steps 1A−2A in Scheme 1; and (iii) by cleavage of O−H and C−H forming the intermediate $^*CH_2CH_2O^*$ (oxametallacycle), represented by step 1B in Scheme 1. These pathways can be interconnected depending on the nature of the metal. Cleavage of the C−C bond of the intermediates is followed by hydrogenation/dehydrogenation of $CH_x{}^*$, water activation and oxidation of C* species.

We start by briefly reviewing the results obtained for ethanol decomposition on clean metal surfaces, and then the findings of experimental and theoretical investigations of SRE are presented.

2.1. Ethanol Decomposition. Spectroscopic studies using clean metal surfaces are important means for identifying intermediates formed during the catalytic reactions or reactant decomposition.[19] In the case of SRE, early studies by Gates et al.[20] showed that ethanol decomposition (eq 3−5) on Ni(111) led to the formation of acetaldehyde, CH_4, CO, H_2, and surface carbon at temperatures between 155 and 500 K, suggesting that bond activation occurs in the order: (1) O−H, (2) CH_2

DOI: 10.1021/cs5020755
ACS Catal. 2015, 5, 3841−3863

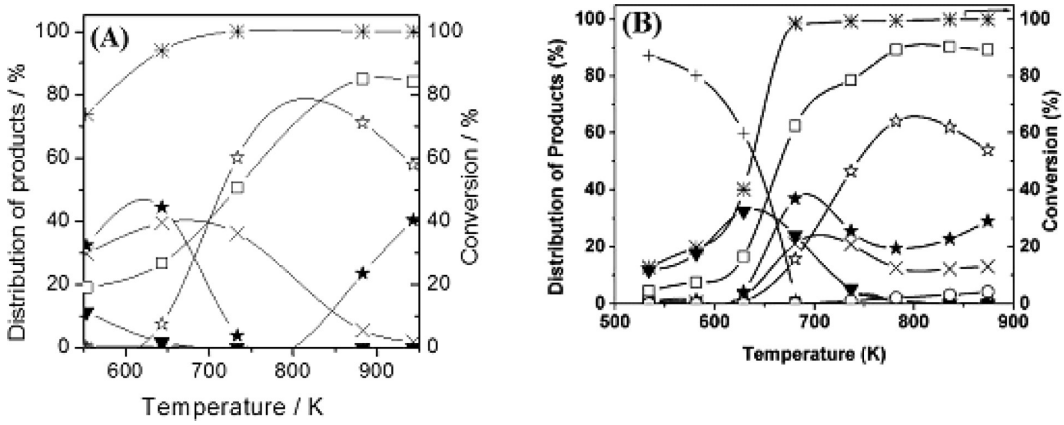

Figure 1. Reaction data for SRE on Ni/Al_2O_3 (A)[6] and Co/SiO_2 (B)[24] after H_2 activation at 623 K. Selectivity (S): ★ S_{CO}, × S_{CH4}, ☆ S_{CO2}, ▼ $S_{acetaldehyde}$, □ S_{H2}, ∗ ethanol conversion, ○ deposited carbon. Reprinted (panel A was adapted in part) with permission from refs 6 and 24. Copyright 2007 and 2009, respectively, Elsevier.

(methylene C−H), (3) C−C, and (4) CH_3 (methyl C−H). This indicates that steps 1−3 in Scheme 1 would better represent the reaction pathway for this catalyst.

$$CH_3CH_2OH \leftrightarrows CH_3CHO + H_2 \quad (3)$$

$$CH_3CHO \leftrightarrows CO + CH_4 \quad (4)$$

$$CH_4 \leftrightarrows C + 2H_2 \quad (5)$$

Experimental Studies of SRE. Experimental studies of SRE carried out on supported Ni[6,21] and Co[13,22−24] catalysts employing a plug-flow reactor described the products that were desorbed as a function of temperature (Figure 1). The results for Ni based catalysts confirmed that ethanol at low temperatures is first dehydrogenated, with desorption of acetaldehyde and H_2 (Figure 1A). By increasing the temperature, in parallel with the desorption of acetaldehyde, it is also observed the C−C bond scission and decomposition of acetaldehyde, resulting in the formation of CH_4, CO, and H_2, with a CO/CH_4 ratio of about one, in temperatures below 610 K. A first analysis of these results suggests that they are consistent with the spectroscopic results previously discussed for Ni(111). However, it is also reasonable to assume that, at temperatures below 700 K, the acetaldehyde formed is dehydrogenated to $*CH_2C*O$ or *CHC*O, followed by C−C bond break yielding CO and CH_x. The latter species would be then hydrogenated to CH_4. In this case, the reaction proceeds though steps 1−7, shown in Scheme 1. By increasing the temperature, the methane concentration decreases and the hydrogen selectivity reaches 100%, which could be due to CH_4 reforming or by suppression of CH_x hydrogenation forming CH_4.

Indeed, a critical step for a selective and stable catalyst is the evolution of the CH_x species forming CH_4 or C* as displayed in Scheme 1, steps 7 and 8, respectively. Accordingly, Jones et al.[25] used DFT (Density Functional Theory) calculations to show that the stabilities of *CH and C* and reaction barriers (*CH + * ⇆ C* + H*) over a Ni surface are strongly dependent on the temperature. Although the decomposition of *CH to *C was favored at high temperature, at low temperature, CH_x hydrogenation would take place yielding CH_4. Further theoretical studies of CH_x species adsorbed on Ni(111),[26] revealed that the highest activation barrier is the H abstraction from methylidyne (*CH) (Figure 2). DFT calculations for Ni(211) and Ni(111) showed that *CH and

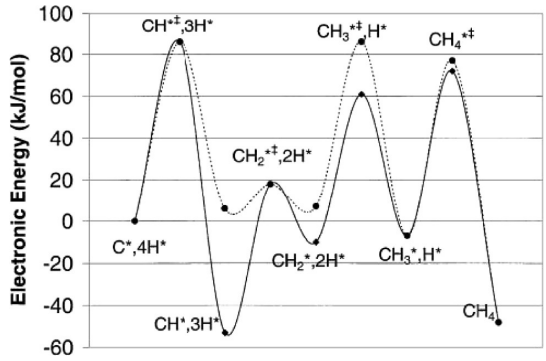

Figure 2. Electronic energy variation of CH_x species and the corresponding activated complexes at each dehydrogenation step on Ni(111): quantum chemical values (◆) and fitted values (●). Reprinted with permission from ref 26. Copyright 2000, Elsevier.

C* were more stable on lower coordination Ni sites (defect sites).[27] Interestingly, the relative stability was strongly sensitive to metal structure, with *CH being more stable than C* on terrace sites, while the opposite behavior was found for step sites. These results strongly suggest that the subsequent hydrogenation of *CH and formation of CH_4, an undesirable parallel reaction, is sensitive to metal structure and is favored on higher coordination metal sites. The oxidation of C* is also critical in SRE, because the carbon accumulation can lead to rapid catalyst deactivation. Carbon can be formed on the surface and in the subsurface layer by different routes, depending on the metal (this issue is discussed in section 3.3). The main challenges in the development of catalysts for SRE concerns the fine-tuning between the ethanol activation, subsequent C* formation, and the removal of the C* species by oxidation as well as the ability to hinder hydrogenation rearrangements of CH_x fragments that form CH_4 at low temperature.

Several theoretical studies have been conduct to address the most plausible ethanol activation pathways according to metal and structure. In the case of Pt, a metal with lower density of states near the Fermi level, Alcalá et al.[28] found that in terms of the stability and reactivity of the ethanol-derived surface species over Pt(111), 1-hydroxyethylidene (CH_3C*OH) and ketenyl (*CHC*O) presented the lowest energy transition states for C−O and C−C bond cleavage, respectively, and at high

DOI: 10.1021/cs5020755
ACS Catal. 2015, 5, 3841−3863

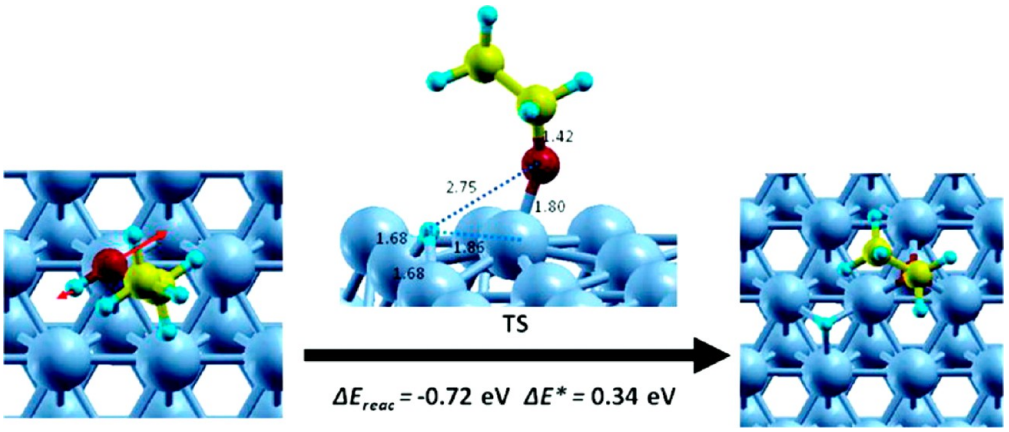

Figure 3. Calculated reaction pathway and transition state structure for 2* + CH_3CH_2OH → CH_3−CH_2−O* + H* on Co(0001) surfaces. The red arrows indicate the possible movement of corresponding species in the reaction step. The marked distances are in Å. Reprinted with permission from ref 34. Copyright 2012, American Chemical Society.

temperatures the C−C bond cleavage should be faster than the C−O. These results are endorsed by the absence products generated by the C−O bond cleavage, such as C_2H_4 and C_2H_6.[28−31] Accordingly, DFT study of ethanol conversion over Pt(111) by Vlachos and co-workers[32] indicates that the initial H abstraction from the α-C−H to form CH_3CH^*OH (step 1A in Scheme 1) would be strongly more favorable thermodynamically over the O−H to form $CH_3CH_2O^*$ (step 1 in Scheme 1); however, considering the activation energy, the authors were not able to determine the predominant pathway. The acetyl (CH_3CO^*) is formed primarily via dehydrogenation of $CH_3CH_2O^*$ or CH_3CH^*OH intermediate (steps 2−3 or 2A−3A in Scheme 1, respectively), and is converted to *CHC*O (steps 4−5, Scheme 1). The significant C−C bond scission occurs from the *CHC*O intermediate. The increasing levels of dehydrogenation have the following as consequence: (i) the increase of the binding energies; (ii) the decrease in the activation energy for the C−C bond cleavage; and (iii) the increase in the activation energy for cleavage of the C−O and C−OH bonds. The C−H bond cleavage would occur before C−C[28] through the formation of ketenyl (*CHC*O) intermediary given methylidyne (*CH) and *CO as products (step 6 in Scheme 1).[32] At high temperatures, dehydrogenation of $*CH_x$ species produces adsorbed carbon (*C) (step 8 in Scheme 1).[29] Therefore, experimental and DFT results suggest that the main reaction pathway for Pt(111) would involve steps 1A−3A followed of steps 4−6 in Scheme 1. The reaction pathway observed for Pt seems to be structure sensitive. For example, for Pt(311), Cong et al.[33] reported a possible mechanism involving the adsorption of ethanol by α-C, followed by cleavage of C−C bonds in a reaction pathway as follows: H* + CH_3CH_2*OH → CH_2*OH + CH_4.

In the case of Co, with a higher density of states near the Fermi level, most experimental results (Figure 1B) point to the formation of acetaldehyde at low temperatures, which is supported by theoretical studies. For example, Ma et al.[34] investigated the reaction mechanism for SRE over the Co(0001) surface. The simulations showed that the ethanol molecule adsorbs preferentially through O on a Co top site yielding adsorbed ethoxy species ($CH_3CH_2O^*$) (Figure 3). The formation of acetaldehyde via the adsorbed ethoxy species was proposed as the rate-determining step. It has been also shown that the direct decomposition of $CH_3CH_2O^*$ to $*CH_3$ and HCHO* is not kinetically feasible due to a high-energy barrier, whereas the dehydrogenation of $CH_3CH_2O^*$ to form CH_3CHO^* prior to C−C scission is kinetically favorable.

Therefore, for Co, computational and experimental results indicate that the reaction proceeds initially through of cleavage of OH bond via steps 1 to 6, shown in Scheme 1. The products formed at low temperatures (below 720 K, Figure 1B) are similar to those obtained for the Ni-based catalyst (Figure 1A), but for Co, the $(CO_2+CO)/CH_4$ ratio was much larger than 1, indicating that abstraction of the H of acetyl species to form $*CH_2C^*O$ or *CHC*O species is favored over an early cleavage of the C−C bond, which is explained by the lower d band occupancy of Co compared to Ni.

The above-mentioned results indicate that the ethanol decomposition over Pt and Co could follow slightly distinct mechanisms. Whereas for Co, the ethanol activation takes place via OH bond cleavage forming ethoxy intermediate ($CH_3CH_2O^*$), for Pt another pathway involving the α-C-H bond forming 1-hydroxyethyl (CH_3CH^*OH) is also accepted. Nevertheless, these pathways are interconnected and the cleavage of C−C bond is favored after formation of *CHC*O intermediate via step 6 in Scheme 1. It seems to be a consensus that the cleavage of the C−O bond energy is too high to be broken over these surfaces.

In the case of Pd, Barteau and co-workers have performed extensive TPD (temperature-programmed desorption) and HREELS (high-resolution electron energy loss spectroscopy) studies,[35−38] suggesting that the ethanol activation proceeded through η^2-acetaldehyde and η^1(C)-acetyl species, which would be a reaction pathway involving the steps 1−3 in Scheme 1.[37,39] However, DFT studies by Li et al.[40] suggest an alternative pathway for ethanol decomposition on Pd (initial activation via step 1A and then following steps 3−6 in Scheme 1): CH_3CH_2OH → CH_3CHOH → CH_3CHO → CH_3CO → CH_2CO → CHCO → CH + CO → CO + H + CH_4 + C.

Recently, Sutton and Vlachos[41] performed DFT calculations on close-packed surfaces of Co, Ni, Pd, Pt, Rh, and Ru and confirmed that over a single-metal surface, dehydrogenation is highly favored and takes place before cleavage of C−C. The dehydrogenation should take place via the α-C-H on the less-oxophilic metals (Pd and Pt) and via the O−H on the more-oxophilic metals (Co, Ni, Rh, and Ru). On the other hand, Wang at al.[42] found that an initial β-C-H bond forming adsorbed $*CH_2CH_2OH$ and $*CH_2CH_2O^*$ dissociation is also feasible.

DOI: 10.1021/cs5020755
ACS Catal. 2015, 5, 3841−3863

Accordingly, for Rh(111)[43] and Ru(0001),[44] the formation of an oxametallacycle intermediate (*CH_2CH_2O*) by β-C-H activation was proposed (step 1B in Scheme 1). The formation of this species was confirmed by TPD and spectroscopy analyses.[44,45] DFT studies on Rh(111) surface suggested that initially the O−H is activated, and the ethoxide species further dehydrogenate to an oxametallacycle species. Further dehydrogenation leads to the formation of *CHC*O, which undergo C−C bond breaking to yield methylidyne (*CH) and CO (steps 2B and 3B in Scheme 1).[46,47] These results are in accordance with experimental data obtained by Sheng et al.[48] who reported that the presence of Rh metal results in a substantial formation of CO at low temperature (310 K), which could be explained by the decomposition of an intermediate such as the oxametallacycle species. These results suggest that for Rh, the SRE pathway involves the steps 1B−4B in Scheme 1. However, different results were found by other authors,[41,49,50] suggesting a pathway passing through acetaldehyde (steps 1−3 in Scheme 1). Although significant amounts of methylidyne (*CH) and ethylidyne (*CCH_3) were found on Rh(111),[49] DFT studies showed that over the Rh(211) surface, acetyl (CH_3C*O) species are formed.[50] These results endorse the possible formation of acetaldehyde as an intermediate. Therefore, further experimental studies are required under reaction conditions to elucidate the reaction mechanism over Rh.

In general, it has been accepted that the ethanol activation would take place at the O−H group. Nevertheless, several recent studies have shown that depending on the metal surface, ethanol can be activated through C−H bonds. The first ethanol activation will be important to determine the main reaction pathway, and therefore, the identification of the dehydrogenated intermediates will bring interesting information to elucidate the pathway for C−C bond breakage. The C−C bond cleavage will typically take place in an intermediate with a high dehydrogenation level. The C−O bond energy is too high in most metal surfaces, and its cleavage is not favorable; however, for the more oxophilic metals, such as Rh and Ru, a significant rate for the C−O bond breaking has been observed leading ethane production.

For all pathways, the ability of the metal to hydrogenate/dehydrogenate the CH_x* species formed by C−C bond scission governs the selectivity to CH_4. The formation of CH_4 at low temperatures is undesirable, because the reforming of CH_4 will only occur at much higher temperatures (typically above 1073 K).[25] This is the case for Ni, for which the formation of CH_4 is strongly favored at low temperatures.[6]

2.2. Water Activation and Oxidation of Adsorbed Carbon Species. Activation of H_2O is a vital step in SRE due to the fundamental role of the *OH species in subsequent oxidation steps. The reactivity of Ni surfaces with H_2O can be low, as observed on Ni(100) and Ni(111) surfaces,[51] or very high on the low-coordination sites of the Ni(211) surface.[27] Bengaard et al.[27] calculated the barriers for the reaction H_2O* + * ⇆ *OH + *H and found 91 and 38 kJ/mol for Ni(111) and Ni(211), respectively. The kinetics of the *OH dissociation step on transition metals has also been examined in several theoretical works,[52−58] and it was shown that both adsorption step and consecutive *OH dissociation depend on the metal type and structure. For example, the energy barriers for the reaction *OH + * ⇆ O* + H* obtained for planar Ni(111) surface and Ni(211) were 96 and 114 kJ/mol, respectively. Because the oxidation of CO depends on the formation and dissociation of HO* species, it will be affected by the metal particle size.

After cleavage of the C−C bond and activation of H_2O at high temperature, the CO adsorbed on the metal is oxidized to form CO_2 (step WGS in Scheme 1) according to the well-known water-gas shift reaction (WGS, eq 6).[59,60] Experimental results for SRE[6,24] on Ni- and Co-based catalysts (Figure 1) indicated that increasing the temperature above 620 and 680 K, respectively, caused intensive CO conversion to CO_2.

$$\text{WGS: } CO + H_2O \leftrightarrows CO_2 + H_2 \quad (6)$$

Similar to CO oxidation, the oxidation of CH_x species on the metal surface proceeds at around 600 K. Experimental results for SRE on Ni-based catalysts indicated a decrease of CH_4 formation at around 620 K, which was attributed to either oxidation of CH_x species or decomposition of *CH_x species to *C and subsequent oxidation to *CO_x.[6] DFT calculations showed that *CH_x species could be oxidized by HO* (eqs 7−10) during SRE on a Co(0001) surface.[34] However, although part of this mechanism (eqs 8−10) is well-established for steam reforming of methanol,[61,62] the first step (eq 7) is not kinetically favored.

$$CH_3* + *OH \leftrightarrows CH_3O* + H* \quad (7)$$

$$CH_3O* + * \leftrightarrows HCHO* + H* \quad (8)$$

$$HCHO* + *OH \leftrightarrows HCOOH* + H* \quad (9)$$

$$HCOOH* + 2* \leftrightarrows CO_2* + 2H* \quad (10)$$

At present, the most widely accepted mechanism for oxidation of CH_x species (eqs 11−13) is via CH_x decomposition to *C, followed by subsequent oxidation to CO (Scheme 1, steps 8−10).[29]

$$*CH \leftrightarrows C* + H* \quad (11)$$

$$C* + O* \leftrightarrows CO* + * \quad (12)$$

$$C* + *OH \leftrightarrows CO* + H* \quad (13)$$

In summary, there are still several open questions related to the reaction mechanism of SRE on different metals that should be addressed both experimentally and theoretically. The right balance of the several steps (i.e., ethanol activation, C−C bond cleavage, oxidation steps, and dehydrogenation/hydrogenation of CH_x species) are critical to optimize the catalyst performance, in particular, its stability against carbon accumulation. In this aspect, the ORE reaction, with addition of O_2, can be an alternative, but as discussed in the next sections, it can also bring new aspects related to metal oxidation and the mechanism pathways.

3. EFFECT OF THE METAL NATURE IN SRE

3.1. Interplay between the Metal Particle Size and Catalyst Behaviors in SRE. The surface of a metal nanoparticle intrinsically contain a large amount of low-coordinated sites such as steps, kinks, and vacancies (broadly classified as defects) that have long been considered as important catalytic sites, because the reactants and intermediaries may bind strongly to these low-coordinated sites helping breaking the chemical bonds readily. The fraction of the low-coordinated atoms increases significantly when the metal particle size decreases, concomitant with the decrease of atoms on terraces. As an example,[63] Figure 4 shows the evolution of the type of surface atom as a function of the metal

DOI: 10.1021/cs5020755
ACS Catal. 2015, 5, 3841−3863

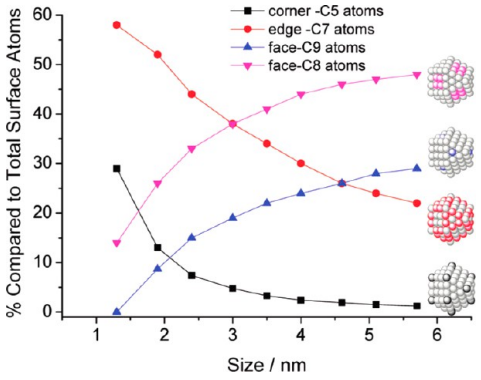

Figure 4. Percentages of different types of surface atoms as a function of particle size. Reprinted with permission from ref 63. Copyright 2012, American Chemical Society.

particle size (for a fcc cuboctahedral nanoparticle, the terraces are either {111} or {100} type). Because the catalytic performance depends on the surface structure of the catalyst under the reaction environment, the interplay among various parameters, such as metal nanoparticle size, shape, and oxidation state as well as reaction conditions are critical.

In the case of SRE, several steps of the reaction mechanism are structure-sensitive, such as the CH_x species dehydrogenation/hydrogenation[27] (steps 7−8, Scheme 1) and the activation of water and oxidation of *C species (steps 8−9, Scheme 1), which are favored on low-coordination metal sites. Therefore, the intrinsic catalytic activity of metal sites located on smaller particles could be different from that on the larger ones, even in the case where no deactivation occurs. In this aspect, undesired reactions such as the hydrogenation of CH_x species forming CH_4 (step 7, Scheme 1) and the growth of carbon filaments during the SRE are favored on higher coordination metal sites. In particular, the growth of carbon filaments requires an ensemble of atoms only found at the terraces and, as a consequence, is favored for particles above a critical size.[64] As a consequence, metal particle size will determine not only catalyst activity and selectivity but also carbon accumulation and graphene growth in SRE. In fact, one of the main challenges to be overcome in SRE is the deactivation of catalysts by carbon accumulation that is briefly discussed in section 3.3.

The metal particle size is also a determining factor in the metal susceptibility to oxidation under reaction conditions. Thus, the catalyst surface can easily change and adopt the structure corresponding to thermodynamic equilibrium that is dependent on the particle size.[65] Although the activation of ethanol via ethoxy species can occur on metallic or oxidized sites, the cleavage of C−H bonds without oxidation of H* species is an exclusive feature of metals, and as a consequence, the oxidation state is also an important parameter in the SRE mechanism.

A great number of publications are found in the literature addressing the catalytic activity dependence on variables such as temperature of calcination, metal loading, or metal precursor as a way to tune the particle size. However, all these variables may modify other parameters of the catalyst, making difficult to directly correlate particle size and catalytic performance.[66−79] Alternative synthetic methods have been explored, aiming to get more control of the metal dispersion when compared to the conventional impregnation. For example, Ribeiro et al.[24] addressed the use of colloidal Co nanoparticles with different sizes (3−8 nm range) supported on SiO_2 and showed that smaller particles were more active to SRE. Recently, da Silva et al.[80] studied the influence of cobalt particle size in SRE using well-dispersed Co nanoparticles deposited on carbon nanofibers. The turnover frequency increased with decreasing Co particle size, which was ascribed to the increasing number of unsaturated cobalt surface atoms. Moreover, the smallest Co particle sizes showed the lowest catalyst deactivation, which was due to a lower amount of carbon deposition and less sintering (see section 3.3).

The lower coordination number in smaller particles should not only lead to a geometrical effect but could also affect considerably the surface electronic properties in the metal nanoparticle and, consequently, the catalytic activity. For example, as mentioned before, *CH and C* species stability was higher for Ni(211) compared to Ni(111), which modifies the catalyst properties for hydrogenation, CO oxidation, and carbon growth.[27] In the case of Rh, computational studies revealed that different species were formed preferentially on Rh(111) or Rh(553).[49] There is a decrease in the C−H dissociation barrier when changing from Rh(111) to Rh(553), favoring the formation of adsorbed carbon in Rh(553).[49] The better ability of Rh (553) to break C−H bond is due to its higher C binding energy and oxygen coverage. Similarly, α-C-H cleavage appears to be more favorable on Pt(311),[33] which affects the ethanol decomposition mechanism if compared to Pt(111).

Therefore, it is important to keep in mind that changes of metal dispersion usually are followed by changes of other properties such as degree of metal reduction and interaction with the support, which result in correlated variables. Despite the limited number of experimental studies correlating directly the metal particle size with catalytic performance in SRE,[14,24,80] undoubtedly this is one of the main parameters of the catalyst to be optimized for each system and reaction conditions.

3.2. Importance of Metal Oxidation State. The outlet stream of SRE is composed of redox atmosphere, and the catalyst may undergo reduction or oxidation during reaction as a function of the catalyst bed position. The reaction of the metal nanoparticle with oxygen is favored by the presence of H_2O or O_2 (in the case of ORE) and in some cases by the interaction with the oxide support, contributing to catalyst deactivation due to suppression of the active metal sites. On the other hand, the formation of reducing agents, such as CO and H_2 during the SRE reaction, contributes to regenerate the active sites.[13]

The redox equilibria and phase stability of transition metal oxides at nanoscale are strongly influenced by the surface energy. The metal redox equilibrium (Metal + O ⇆ Metal—O) depends on the free energy, and it has been shown that the oxidation is favored by decreasing both the metal particle size and the temperature.[65] Spinel phases, such as Co_3O_4, $MgAl_2O_4$ or Fe_3O_4, have lower surface energies than other oxides of the same metal. For example, the calculated Co−O phase diagram of 10 nm nanoparticles shows a much diminished stability for the divalent oxide (surface energy of 3.57 J/m^2).[65] Therefore, under reaction conditions, the Co^{2+}/Co^0 ratio could be controlled, in principle, by manipulating composition of reactants and temperature, as well as by manipulating the Co cluster sizes. The understanding of the redox equilibria of metal nanoparticles is therefore an important point.

It is known that small metal nanparticles are less stable than bulk metal due to the significant contribution of the surface

DOI: 10.1021/cs5020755
ACS Catal. 2015, 5, 3841−3863

energy. For example, the surface energy of cobalt metal nanoparticles has been estimated from the number of broken Co−Co bonds on the particle size. The thermodynamic approach was employed by van Steen et al.[81] to evaluate the stability of cobalt metallic nanocrystals in water/hydrogen mixture. The thermodynamic calculations showed that spherical cobalt crystallites with a diameter less than 4.4 nm are unstable and readily reoxidized to CoO under realistic Fischer−Tropsch synthesis conditions (P_{H_2O}/P_{H_2} < 1.5, T = 493 K).[81] For SRE, in which a larger amount of H_2 is formed even at moderate conversions, the oxidation threshold should occur at much smaller size. Accordingly, Luo et al.[82] performed ab initio thermodynamics studies on CoO surfaces and suggested that under SRE, the presence of a reducible oxide may be necessary to stabilize Co^{2+}. However, as pointed out by Zheng et al.,[83] kinetic barriers may trap metastable phases, and a deep evaluation of the impact of the reaction conditions on the metal oxidation state has to be done.

From the experimental point of view, the influence of metal oxidation state on the activity and selectivity to H_2 in SRE and ORE over metal-based catalysts has been reported.[13] The catalyst deactivation and decrease in selectivity to H_2 during ORE over Co- or Ni-based catalysts was attributed to the oxidation of the surface of Ni or Co particles by oxygen from the feed.[84−86] In this aspect, the addition of noble metals in supported Co and Ni catalysts[70] has been shown to play a significant role in stabilizing the metallic phase increasing the performance of the catalysts (this will be discussed in section 4).

So far, most of the studies have been dedicated to understand Co-containing systems, and for sake of simplicity, we will restrict the discussion about the role of the metal oxidation state in this system. Several similar and interesting aspects discussed for Co are also expected for other metals, in particular in the more oxophilic ones. The two most common crystalline phases of cobalt oxides are CoO and Co_3O_4, both showing interesting electronic and magnetic properties in a wide variety of scientific and technologies applications. The most common catalyst precursor is Co_3O_4, which is activated in hydrogen before reaction. The transformation mechanism among various cobalt oxides in hydrogen or in oxygen atmosphere is therefore of a great importance and intrinsically related to the formation of the active species of the catalyst as well as to the regulation of the dispersion degree and structure, according to the reaction conditions.

Potoczna-Petru and Kepinski[87] showed that the reduction of Co_3O_4 to metallic Co proceeds in two steps via rocksalt CoO phase (r-CoO) formation. Based on electron microscopy analysis, it was found that the degree of reduction of Co_3O_4 strongly depends on the particle size and morphology, which were determined by the pretreatment conditions. For the smallest particle (5.3 nm), the reduction to metallic Co proceeds directly at low temperature (573 K). However, for bigger particles (12.1 and 20.3 nm), coexisting phases of Co, CoO, and Co_3O_4 were detected at temperature interval of 573−773 K. It has been proposed that the reduction is controlled by the surface defect concentration, which facilitates the reduction process. More recently, Nam et al.[88] showed that kinetic control conditions (rapid heating at high temperatures) during preparation of pure oxide nanocrystals (>20 nm) could produce a metastable wurtizite-oxide phase (w-CoO), while thermodynamic control conditions (prolonged heating at lower temperatures) produce the r-CoO. During the oxidation process, w-CoO phase was converted into Co_3O_4 phase via formation of r-CoO phase, but the r-CoO phase was directly oxidized to Co_3O_4.

Interesting results about surface reactivity of Co nanoparticles and Co(0001) single crystal toward H_2 and O_2 atmospheres were obtained by Papaefthimiou et al.[89] by combining ambient pressure photoelectron spectroscopy and in situ X-ray absorption fine structure spectroscopy (XAFS) data. The Co nanoparticles supported on a thick amorphous carbon film were prepared by the low-energy cluster deposition technique. The authors clearly showed that the redox behavior of Co was drastically modified due to size effects. Contrary to the stable r-CoO and Co_3O_4 spinel phases that exist in the bulk oxides, Co nanoparticles contained a significant portion of a metastable w-CoO that was more difficult to be reduced or oxidized (Figure 5). The possible reason for this difficulty is the

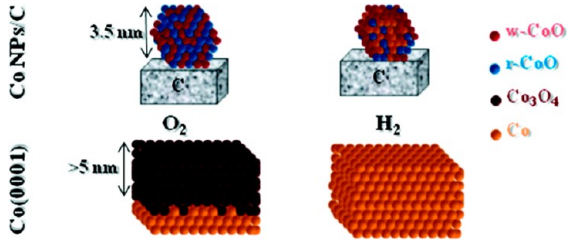

Figure 5. Schematic representation of redox behavior of a 3.5 nm Co nanoparticles supported on amorphous carbon compared to a Co(0001) crystal surface, at 520 K. Reprinted with permission from ref 89. Copyright 2011, American Chemical Society.

structural transformation that has to take place to transform w-CoO to Co_3O_4 or Co metal.[89] Although the driving force to stabilized the w-CoO phase in the Co nanoparticles was not fully understood by the authors, it was suggested that it could be related to the presence of traces of diluted surface carbon that may have stabilized metastable surface structures.[90] In fact, earlier studies[91] on colloidal Co nanoparticles showed that smaller particles were easier to be reduced compared to the larger ones. The important point clarified by these works is that the redox equilibrium in nanoparticles can be determined by high kinetic barriers related to structural phase transformations, induced or not by the interaction with the support and that they will be dependent on the particle size.

Another example was given by Avila-Neto et al.,[13] in which they used temperature-resolved XANES-H_2 (X-ray absorption near edge structure) to elucidate the phase transformation of Co-based catalysts supported on different oxides (Al_2O_3, CeO_2−Al_2O_3 and La_2O_3−Al_2O_3) as a function of reducing temperature. It was shown that a two-step reduction process occurred for all catalysts: $Co_3O_4 \rightarrow CoO \rightarrow Co^0$, but the temperature threshold depends on the support. The faster reduction of Co_3O_4 to CoO and the higher maximum of CoO concentration achieved for Co/La_2O_3−Al_2O_3 and Co/CeO_2−Al_2O_3 reflected the lower interaction of Co_3O_4 with these supports compared to Al_2O_3.

As shown above, the stability against oxidation/reduction of the nanoparticles, exemplified for Co, is affected by the nature of the nanoparticle (such as size and composition), interaction with support, and reaction conditions. As a consequence, it is highly desirable to characterize the catalysts under operando[92,93] conditions to obtain structural and electronic

DOI: 10.1021/cs5020755
ACS Catal. 2015, 5, 3841−3863

information simultaneously with activity/selectivity measurements. SRE and ORE have been studied in situ or operando conditions using different characterization techniques.

Martono and Vohs[94] evaluated ethanol reaction on model Co/YSZ(100) (YSZ = yttria-stabilized ZrO_2) catalysts and found that whereas metallic Co sites promoted ethanol decarbonylation producing CO, H_2, and adsorbed CH_3 species, the presence of oxygen adatoms on metallic Co favored the formation of acetaldehyde as schematized in Figure 6. These

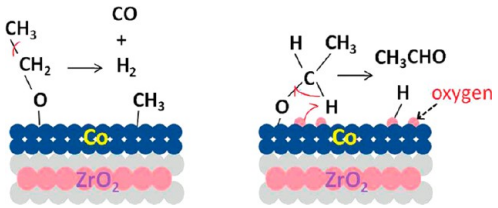

Figure 6. Schematic diagrams showing the ethanol reaction over metallic cobalt and oxygen-covered metallic Co. Reprinted with permission from ref 94. Copyright 2011, American Chemical Society.

results indicated that the presence of adsorbed O atoms on the metal surface can increase the activity to ethanol dehydrogenation, and as a consequence, an increasing metal coverage with intermediates of adsorption of acetaldehyde is expected. In contrast, the ethanol dehydrogenation on CoO was much less reactive than metallic or oxygen-covered cobalt, suggesting that adsorbed oxygen plays an important role in this reaction.

It is worthwhile to mention that from the theoretical point of view, the density of O and OH species on the metal surface is correlated with the free energy of these species, which have been calculated in typical conditions of steam reforming.[25] The density of O and OH species is expected to decrease in the following order: Co > Ru > Rh > Ni ≫ Pt ≫ Pd. Depending on the steam-reforming conditions, especially for Co and Ru, the high O and OH species coverage can oxidize the metal surface, which would change the main dehydrogenation pathway.

The metal redox equilibrium has been mainly addressed experimentally on Co-based catalysts, and metallic Co and Co^{2+} species have been detected under SRE through different techniques, such as magnetic measurements, in situ XRD (X-ray diffraction), and in situ XAFS. Llorca et al.[95] investigated various supported cobalt catalysts (Co/MgO, Co/Al_2O_3, Co/SiO_2, Co/TiO_2, Co/V_2O_5, Co/ZnO, Co/La_2O_3, Co/CeO_2, and Co/Sm_2O_3) by magnetic measurements by submitting the catalyst to SRE and then transfer to the magnetic measurements without exposition to air. The authors detected both Co and Co^{2+} species and suggested that both coexist under reaction conditions. de la Peña O'Shea at al.[96] investigated the evolution of nanometric Co_3O_4 (~21 nm) by in situ XRD and observed that while Co_3O_4 is active for dehydrogenation of ethanol, leading to acetaldehyde, CoO and Co^0, which are formed under reaction conditions at higher temperatures (>573 K), are the active species in SRE.

The catalytic roles of Co^0 and Co^{2+} in SRE pathways were investigated in more detail on Co/MgO catalysts.[97] The $Co^0/(Co^0+Co^{2+})$ fraction was varied using different calcination and reducing treatments. The reaction pathways during SRE were shown to be different on Co^0 and Co^{2+}. Co^0 was much more active than Co^{2+} for ethanol conversion, C−C cleavage, and WGS reaction, whereas formation of CH_4 was enhanced on Co^{2+}. Minimization of Co^{2+} species and stabilization of Co^0 against oxidation were crucial to achieve a high H_2 productivity and yield.

Similar results were obtained by Lebarbier et al.[98] by addressing the effect of Zn promoter in the Co^0/Co^{2+} ratio of Co/ZrO_2 catalysts through different characterization methods. It was shown that addition of Zn inhibits the oxidation of metallic cobalt particles by H_2O leading to a higher Co^0/Co^{2+} ratio, which promotes the ethanol conversion through dehydrogenation. In addition, it was found that Co^{2+} plays a major role in the CH_4 formation and that the degree of CH_4 formation can be lowered by inhibition of Co oxidation with Zn.

Avila-Neto et al.[13] showed that for Co-supported catalysts on both SRE and ORE, the rate of carbon deposition depends on the degree of oxidation of the Co particle (Figure 7). A linear

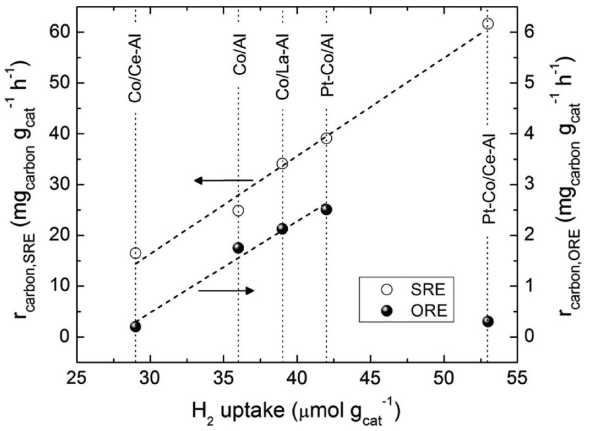

Figure 7. Correlation of carbon deposition with H_2 uptake (degree of Co reduction) of Co supported catalysts under SRE and ORE. The oxides supports, Al_2O_3, CeO_2-Al_2O_3, and La_2O_3−Al_2O_3, were abbreviated as Al, Ce-Al, and La-Al, respectively. Reproduced with permission from ref 13. Copyright 2012, Elsevier.

behavior between oxidation degree of the Co particle (the higher H_2 uptake, the more reduced is the particle) and rate of carbon deposition was observed. Carbon deposition mechanisms are discussed in more detail in section 3.3. Concerning the metal oxidation state, by performing in situ XANES, the authors showed the evolution of the oxidation state as a function of temperature under reaction conditions. After reduction and exposition to reactants of SRE or ORE at low temperature (373 K), all tested catalysts were partially oxidized, showing about 20−25% of Co^{2+} (Figure 8). The oxidation further proceeded by increasing the temperature due to the presence of H_2O reaching a maximum oxidation of about 50% of Co^{2+} at around 573 K. Above this temperature, the fraction of metallic Co increased, indicating the reduction of the catalyst by ethanol, reaching a maximum at 733 K. Under ORE, the oxidation was more aggressive, with maximum oxidation degree around 90% at 673 K. The fraction of metallic Co under reaction conditions depended on the nature of support and on the presence of Pt, following the order of Co/Al < Co/Ce−Al < Pt−Co/Ce−Al (Figure 8D). By analyzing the reaction outlet by mass spectrometry, it was shown that ethanol undergoes oxidative dehydrogenation at low temperature, whereas the reforming products (H_2, CO and CO_2) were observed at temperatures higher than 623 K (Figure 8C). These results correlate well with the evolution of metal oxidation state.

DOI: 10.1021/cs5020755
ACS Catal. 2015, 5, 3841−3863

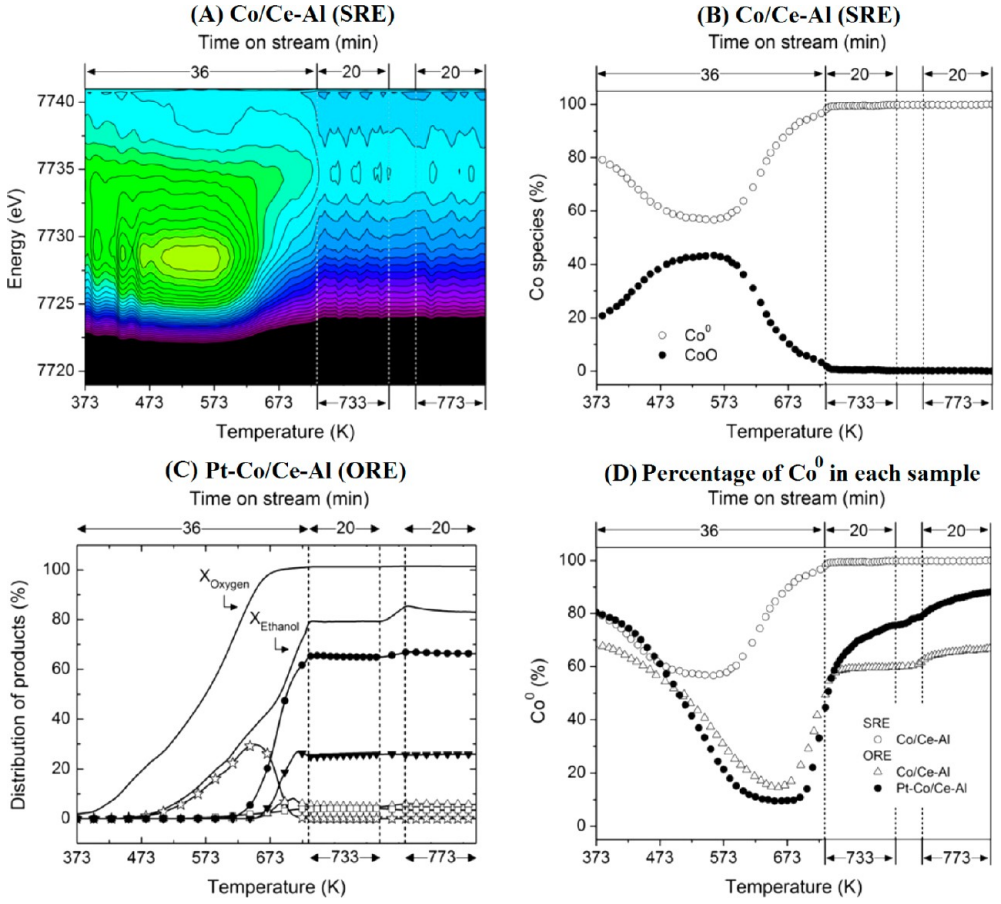

Figure 8. (A) Temperature-resolved XANES-SRE spectra of Co/Ce−Al and (B) evolution of Co species as a function of temperature in this sample. The absorption intensity in (A) increases from lighter to darker color. (C) Effluent composition of the reactor for Pt-Co/Ce-Al under ORE (X_i − conversion, ● H_2, ▼ CO_2, ☆ acetaldehyde, □ CH_4, Δ CO). (D) Evolution of Co species as a function of temperature under SRE and ORE for different catalysts. Adapted with permission from ref 13. Copyright 2012, Elsevier.

The results presented above clearly point out that both metal and oxidized species play very important roles during SRE or ORE, and this finding motivates a deeper discussion about the nature of the active sites for ethanol reforming and how they affect the reaction mechanism. In this aspect, an important point already mentioned is how the metal redox equilibrium affects the carbon deposition, a major issue for SRE. Therefore, to obtain an optimized catalyst for SRE, the interplay between metallic and oxide states and their fine-tuning seems to be critical. The studies on Co nanoparticles showed that coverage of O and OH species or a high oxidation degree changes the dehydrogenation mechanism, and the acetaldehyde formation can be favored. On the other hand, at these conditions, the metallic surface sites can be blocked, diminishing the catalyst activity for further reforming of the intermediates and C−C bond cleavage. At low temperature, Co tends to be more oxidized compared to Ni, and therefore, the main product for ethanol conversion over Co is acetaldehyde while CO and CH_4 are formed over Ni (Figure 1).

3.3. Carbon Accumulation in SRE. One of the main challenges in SRE is the control of carbon deposition on the metal surface, which is a fundamental requirement for a stable and active catalyst. A great number of experimental and theoretical studies have addressed the deactivation problem in reforming of hydrocarbon, especially for Ni-based catalysts. The main pathway leading to carbon atoms formation on the catalyst surface in SRE is the CH_x decomposition to *C (step 8 in Scheme 1). The steps of oxidation of C* and activation of ethanol should then be equilibrated to avoid carbon accumulation on the metal surface (step 10 in Scheme 1).

Three forms of chemisorbed carbon on Ni-based catalyst have been distinguished: on-surface carbon, subsurface carbon, and graphene islands.[99] It has been shown for Ni catalysts that graphene is thermodynamically the most stable form. Between the other two forms, subsurface carbon is thermodynamically more stable than on-surface carbon, and its formation depends on the energy involved in the carbon diffusion to a subsurface.[99,100] At a high carbon coverage on the metal surface, migration to subsurface takes place (i.e., carbon diffuses partially to subsurface positions or to bulk positions), which modifies the nature of the sites on the surface.[99] The surface and subsurface carbon have a great influence on the stability of adsorbed species and thus on the reaction kinetics. TEM (transmission electron microscopy) studies[101−108] of carbon deposition on 3d transition-metal-based catalysts (i.e., Ni, Co, Fe) showed that after metal saturation, the carbon segregates to the metal surface, initiating the graphene formation. A surface diffusion mechanism has also been proposed for carbon deposition on the metal surface.[108,109]

The initial stage in the mechanism of graphene growth on transition-metal surfaces was studied by DFT calculations.[27,108] It was proposed that graphene growth proceeds via a step-flow mode on face-centered cubic (fcc) and hexagonal closed-packed (hcp) metal surface of Ni and Co; that is, the step edges

DOI: 10.1021/cs5020755
ACS Catal. 2015, 5, 3841−3863

on both metal surfaces may act as preferential nucleation sites for graphene growth. Contrarily, on Rh, Ru, and strained Ni, an unstable and finite graphene layer is formed, indicating that the carbon nucleation is energetically unfavorable in these surfaces.[27,108] These results were related to the different match of metal lattice in each case with the graphene lattice. Although for Ni, the match is very closed, for Ru, Rh, and strained Ni, the metal lattice is too large, and the graphene formation is hindered. The similar results found for Ru, Rh, and strained Ni indicate that the geometric effect was more important than the electronic one.

As mentioned above, the bulk solubility and diffusion of carbon atoms play a critical role in the carbon formation on the surface of 3d transition metals, which is not applicable to noble metals due to the very low solubility of carbon in these metals.[110] Peng and coauthors[111] examined the effect of the shape and particle size on the growth of graphene layers on MgO-supported Pt nanoparticles. In contrast to the observations for graphene growth on Ni nanoparticles,[104] the Pt particles retain their compact and faceted shape during carbon accumulation. It was shown that graphene layer growth on Pt particles is strongly dependent on Pt particle size, as is schematically illustrated in Figure 9.

The results above clearly show that the formation of graphene layers and carbon filaments on the catalyst surface under reaction conditions depend on the nature of the metal and its particle size. The control of carbon accumulation depends on the availability of surface oxygen required to oxidize the *C species. Therefore, the equilibrium between ethanol activation and carbon removal is a key point to be found. Under SRE, the presence of reactants with high redox potential such as H_2, CO, and H_2O (and O_2 in ORE) as well as the metal−support interaction will tune the availability of surface oxygen according to the gas composition, temperature, and metal particle size. In fact, the metal nature and particle size impacts not only on the oxidation state of the metal but also on the type of carbon that is formed.

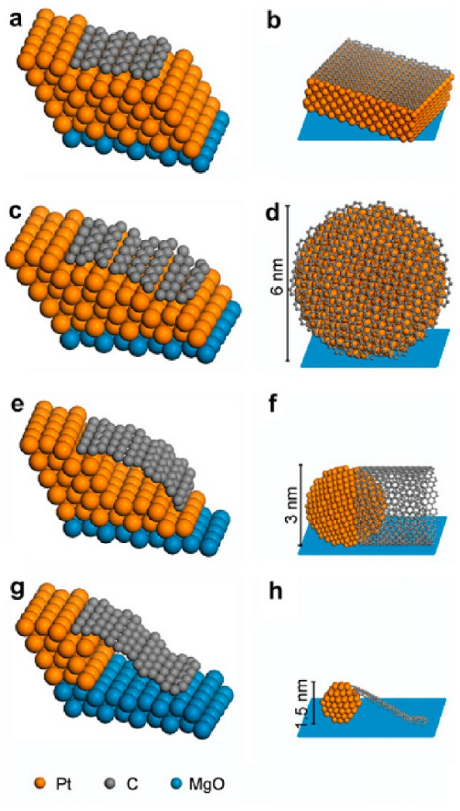

Figure 9. Schematic illustration of the impact of particle size on the growth of graphene on Pt/MgO: (a and b) graphene layer on (111) Pt surface; growth initiated at a [101] step; (c and d) encapsulation of large Pt particles (~6 nm) by graphene; (e and f) growth of nanotubes from medium Pt particles (~2−6 nm); (g and h) formation of graphene layer on small particles (<2 nm) that migrates to the support. Reprinted with permission from ref 111. Copyright 2012, Elsevier.

For example, Chen et al.[74] showed the dependence of carbon accumulation on metal particle size under ORE by studying the Ni-based catalyst obtained from reduction of $LaNiO_3$ perovskite or by impregnation of a Ni precursor on La_2O_3 (10 and 23.9 wt %). The results presented in Figure 10a−f show that the resistance to carbon accumulation is higher on the $LaNiO_3$-derived catalyst due to the higher dispersion of Ni. Accordingly, it has been suggested that the carbon deposition rate is minimized for Ni particles with sizes below 10 nm.[112] Moreover, for the Ni/La_2O_3 catalyst synthesized by impregnation, a significant formation of carbon filaments/nanotubes and graphitic carbon covering the Ni particles was observed .

Cobalt catalysts also displayed an effect of the particles sizes in the carbon accumulation. For example, Ribeiro et al.[24] showed that the average rates of deposited carbon under SRE decrease from 0.010 to 0.002 g carbon h^{-1} by decreasing the Co nanoparticle mean diameter from 7.8 to 3.2 nm on model $Co-SiO_2$ supported catalysts. Similar size dependence was found by da Silva et al.[86] on Co particles supported on carbon nanofibers. Soykal et al.[113] carried out SRE over Co/CeO_2 catalysts with two different CeO_2 particle sizes, 95 nm (Co/CeO_2(MP)) and 6.5 nm (Co/CeO_2(NP)). The smaller size of the support particle in Co/CeO_2(NP) led to a better Co dispersion. As shown in Figure 11A, significant loss of activity within 12 h was observed for Co/CeO_2(MP), accompanied by pressure buildup in the reactor, suggesting carbon accumulation. TEM images (Figure 11B) show the formation of different carbon types on the metal surface: the larger Co particles (about 25 nm) in Co/CeO_2(MP) favor the formation of carbon filaments while the smaller ones (about 5 nm) in Co/CeO_2(NP) lead to the encapsulation by a carbon layer. The authors claimed that a combination of factors lead to the difference in performances not only related to the metal but also to the support. In fact, da Silva et al.[86] pointed out that smaller Co particles (<4 nm) tend to deactivate under ORE condition due to oxidation of the metal rather than carbon accumulation.

These results presented above briefly illustrate several aspects of catalyst and reaction conditions that impact on carbon accumulation and should be tackled.

4. IMPORTANCE OF THE METAL SURFACE ELECTRONIC PROPERTIES MODIFIED BY ALLOY FORMATION TO OBTAIN A BALANCED AND STABLE CATALYST

The use of bimetallic catalysts is a strategic option to modify the electronic properties of metal surfaces[114−119] and successful examples can be found in several catalytic processes.[120−123] However, despite the efforts undertook to understand structure and properties of bimetallic catalysts, there is a broad set of variables that could be deeply explored concerning the specific

DOI: 10.1021/cs5020755
ACS Catal. 2015, 5, 3841−3863

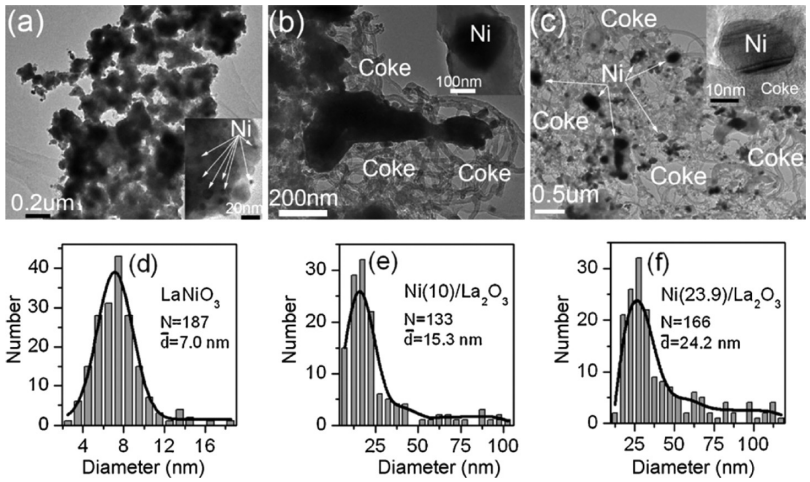

Figure 10. Transmission electron microscopy images and corresponding particle size distribution of Ni-based catalysts after ORE reaction: (a) and (d) reduced $LaNiO_3$ perovskite, (b) and (e) 10 wt % Ni impregnated on La_2O_3, and (c) and (f) 23.9 wt % Ni impregnated on La_2O_3. Reprinted with permission from ref 74. Copyright 2012, Elsevier.

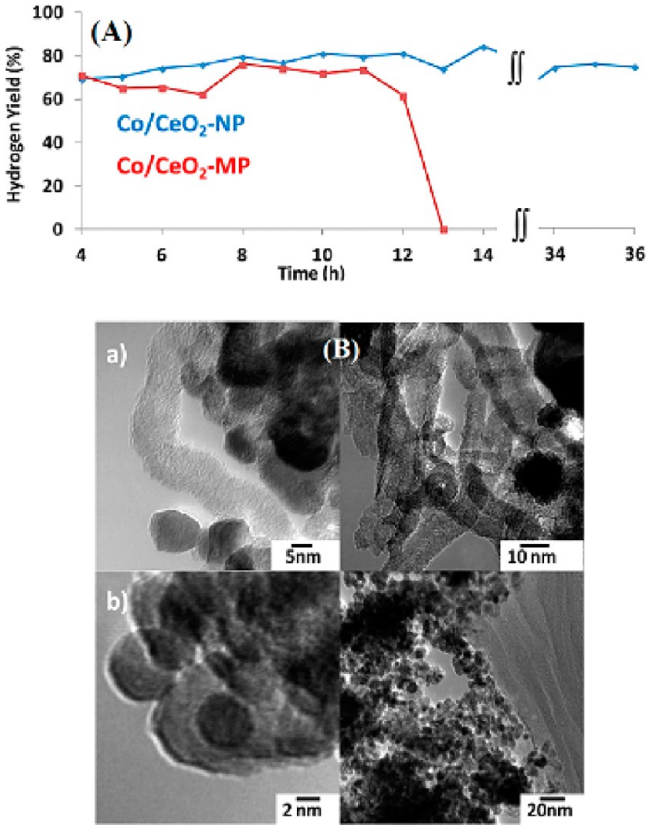

Figure 11. (A) Time-on-stream performance of Co/CeO_2(MP) and Co/CeO_2(NP) during SRE (MP = micrometric CeO_2 particles; NP = nanometric CeO_2 particles). (B) TEM images showing the carbon species deposit under SRE (a) Co/CeO_2(MP) and (b) Co/CeO_2(NP). Reprinted with permission from ref 113. Copyright 2012, American Chemical Society.

conditions of SRE and ORE. The addition of promoters has been extensively studied in the reforming of hydrocarbons as a mechanism to avoid carbon accumulation with time on stream. For example, Besenbacher et al.[5] and a recent review by Wei et al.[124] addressed the use of bimetallic catalysts for H_2 production in reforming of hydrocarbons. It is well-known that Ni surface modified with Au or Ag increases the stability of the catalyst.[5,125,126] The presence of Au or Ag over Ni surface decreases the d-band center, decreasing the activation of methane relative to H_2O, increases the reactivity of C* and avoids carbon accumulation. However, similar bimetallic Ag−Ni catalysts did not show higher performance in SRE, probably due to the higher reactivity of ethanol relative to methane.[6]

Sutton and Vlachos[41] evaluated the ethanol activation in several metals and reported a linear trend between the O binding energy to the metal and the activation energy to break the β-C−H, C−C, C−O, and C−O(H) bonds (Figure 12).

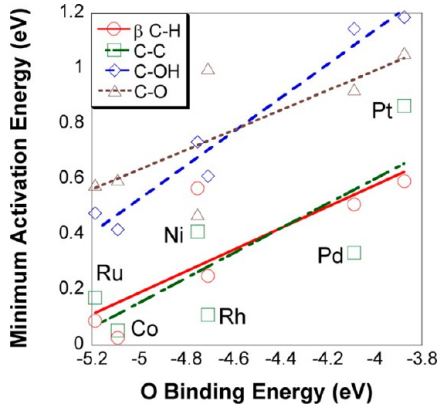

Figure 12. Trends in minimum activation energies for β-C−H, C−C, C−O and C−O(H) bond break, as a function of O atomic binding energy in a series of different metal surfaces. Reprinted with permission from ref 41. Copyright 2015, American Chemical Society.

Even though these results are presented for single metals, it allows inferring about the reactivity of these intermediates in alloys.[123] For example, by alloying Ni and Co it could be expected changes in the catalytic properties compared to Ni, such as (i) increase in O binding energy, leading to a higher O coverage on the metal surface; and (ii) decrease in the minimum activation energy for β-C−H, C−C, C−O and C−O(H) break. However, the main reaction pathway should not change in the NiCo alloy, since both Ni and Co reacts with ethanol through a similar pathway. Contrarily, if Ni is alloyed to Pt or Pd, for example, it is reasonable to suppose that the main

DOI: 10.1021/cs5020755
ACS Catal. 2015, 5, 3841−3863

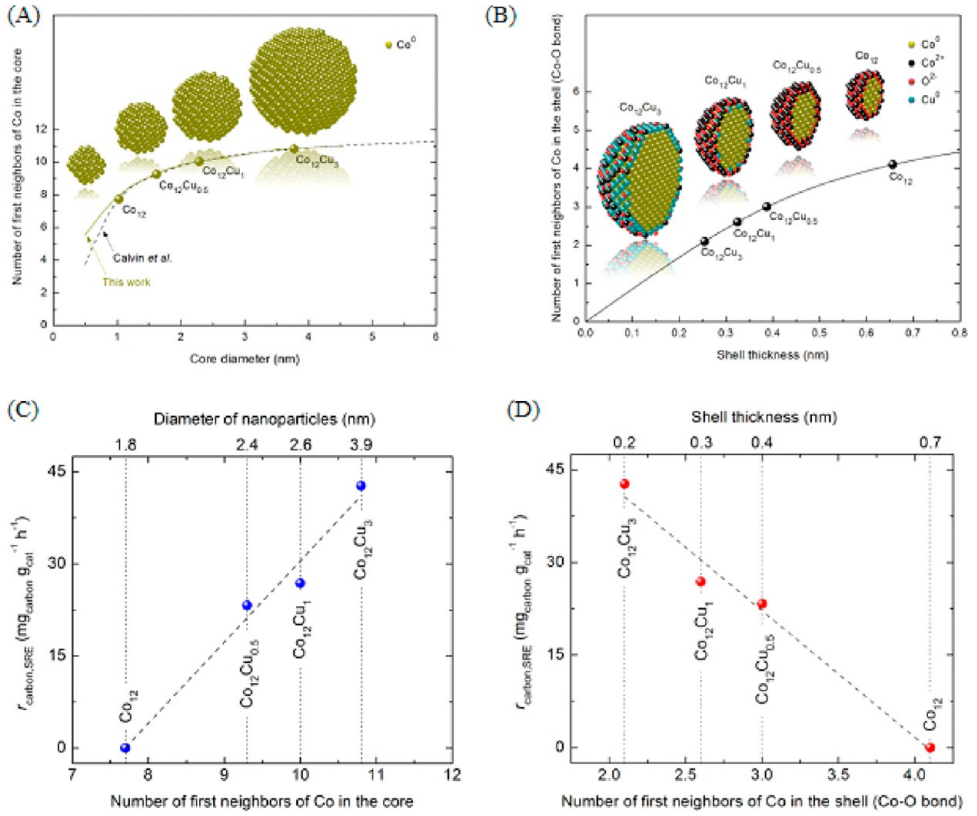

Figure 13. Effect of Cu addition to $Co_{12}/MgAl_2O_4$ (A) number of first neighbors of Co−Co in a fcc cuboctahedral Co core as a function of core diameter, obtained by EXAFS and (B) number of first neighbors of Co−O in a face-centered cubic cuboctahedral shell, as a function of shell thickness, obtained by EXAFS. (C) and (D) Rate of carbon accumulation under SRE (H_2O/ethanol = 12, T = 823 K) as a function of number of first neighbors of Co in the core (C), and number of first neighbors of Co−O in the shell of $Co_{12}Cu_x$ nanoparticles (D). The corresponding estimated core diameters and shell thicknesses are shown in the top axis. Reprinted with permission from ref 130. Copyright 2013, Elsevier. The dashed line in (A) correspond to the dependence of coordination number with the diameter of a nanoparticle based on the work by Calvin et al.[131]

pathway will be correlated with the nature of the alloy formed at surface.

For example, high reforming activity on Ni−Pt catalysts was found by Skoplyak et al.[115] who showed that the Ni−Pt−Pt(111) surface with an upper monolayer of Ni presents greater reforming activity than Pt(111), thick Ni/Pt(111), or a surface with a subsurface monolayer of Pt−Ni−Pt(111). This behavior was explained by DFT calculations, which indicated that the presence of a Ni surface monolayer on Pt(111) shifts the surface d-band center closer to the Fermi level, increasing the interactions with adsorbates. In addition, it was shown that the upward shift in the d-band of the 3d−Pt-Pt(111) surface increases as the 3d metal moved to the left of the periodic table. DFT modeling studies reveled similar results for Fe−Pt−Pt(111) and Ti−Pt−Pt(111) alloys.[31,115,127,128] Also, Sanchez-Sanchez et al.[116] used DRIFTS-MS (diffuse reflectance infrared Fourier transform spectroscopy couple to mass spectrometry) analyses to investigate ethanol decomposition and SRE on Pt, Ni, and PtNi supported on γ-Al_2O_3, and found higher catalytic activity for the bimetallic catalyst.

By alloying metals that results in d-band upward shift, such as Ni−Pt and Co−Ni, a stronger bonding of adsorbates and an increase in activity toward cleavage of C−C and C−H bonds of ethanol relative to monometallic Co and Ni is expected. The opposite is expected in alloys in which the d-band center is shifted downward, such as Cu−Co, Cu−Ni, and Pt−Co. Nevertheless, the impact of d-band shift on carbon accumulation is still not clear because it also depends on the relative activity to the carbon oxidation by H_2O.

For example, in the case of bimetallic Cu−Co supported catalysts, in a catalyst with Cu/Co molar ratio of 0.25, the presence of Cu favored the desorption of acetaldehyde, leading to a reduction in the activity toward C−C bond cleavage.[129,130] For this catalyst, the Cu/Co molar ratio at the surface was about 40 times larger than the nominal concentration. An interesting result found in the Cu−Co system was the correlation of the carbon accumulation ratio with the Cu contents. Despite the enrichment of Cu on the Co surface in all catalysts, found by XPS (X-ray photoelectron spectroscopy), EXAFS (extended X-ray absorption fine structure) results indicated the alloying of Cu−Co and showed an increase in the Co−Co coordination number with Cu content (Figure 13A). This was associated with an increase in the metal particle size when Cu was added to Co, with an apparent correlation between metal particle size and carbon accumulation during SRE (Figure 13C). However, the redox properties of the catalyst also changed by Cu addition, whereas the presence of Cu led to a lower degree of Co oxidation (Figure 13B), modifying its reactivity toward oxidation reactions. The high sensitivity of the amount of oxidized species to the reaction conditions suggests that a shell layer was formed on a reduced core, as illustrated schematically in Figure 13B. The correlation of the rate of carbon accumulation during SRE with the number of first neighbors of Co−O in the shell of $Co_{12}Cu_x$ nanoparticles (Figure 13D) suggests that carbon deposition

DOI: 10.1021/cs5020755
ACS Catal. 2015, 5, 3841−3863

decreased with increase of Co−O species. The chemical composition of the surface therefore determined the electronic properties, with the thickness of the shell formed on a reduced core controlling the density and reactivity of metal−metal oxide on the surface.

Bimetallic Cu−Ni catalysts are one of the most studied bimetallic systems for SRE.[67,132−140] Nevertheless, different conclusions have been reached concerning the use of Cu−Ni catalysts for SRE and ORE. For example, Vizcaino et al.[67] reported that in SRE, the WGS reaction was promoted by the addition of Cu in Ni catalysts. Biswas and Kunzru[138] also reported that the addition of Cu to a Ni/CeO_2-ZrO_2 catalyst resulted in higher activity for WGS as well as for CH_3CHO decomposition and reforming reactions. Velu et al.[140] showed that in the case of ORE, using CuNiZnAl mixed oxide catalysts, the Cu-rich catalysts favored the dehydrogenation of ethanol to CH_3CHO (steps 1−2 in Scheme 1), but the reforming reaction was enhanced by the presence of Ni.

Casanovas et al.[141] used Pd/SiO_2 and Pd/ZnO in the SRE and ORE in the temperature range of 548−723 K to show the formation of PdZn alloy under reaction. On Pd/SiO_2, H_2, CO, and CH_4 were observed during both reactions, suggesting that the decomposition of ethanol or acetaldehyde (eqs 3−4) was the main reaction during SRE or ORE. On the contrary, H_2, CO_2, CH_4, acetaldehyde, and dimethylketone were observed on Pd/ZnO, suggesting a steam-reforming mechanism for both reactions, which occurred on the PdZn alloy. The formation of PdZn alloy during SRE and ORE was showed by HRTEM (high-resolution TEM) and XRD. The authors attributed the formation of acetaldehyde by dehydrogenation of ethanol (steps 1−2 in Scheme 1) and the formation of dimethylketone via acetaldehyde condensation in basic surface sites on ZnO. These results are in agreement with the work by Jeroro et al.,[142] in which TPD and HREELS were used to study the adsorption and reaction of ethanol and acetaldehyde on two-dimensional PdZn alloys deposit on Pd(111), and they found a decrease in the dehydrogenation activity of PdZn alloy and an increase in the barrier for C−H bond cleavage in adsorbed alkoxide and aldehyde intermediates.

It is known that the addition of noble metals, such as Rh, Ru, and Pt, in small amount (0.01 wt %) to Co-supported catalysts[13,85] increases both the degree of reduction of Co and the catalytic activity during SRE and ORE, while the catalyst becomes more susceptible to carbon accumulation. Similar to the results obtained for the noble metals, the addition of Cu to supported Co or Ni catalysts, as discussed above, increases the degree of reduction of Ni or Co, compared to the monometallic systems, which is reflected in higher carbon accumulation during SRE.[129] The increase in the degree of reduction could be explained by the possibility of H_2 to be dissociated on Cu or Pt surfaces producing H atoms, which spillover to Co-oxides.[143] However, at high Pt contents, Zheng et al.[83] demonstrated the complex correlation between oxidation state and atmosphere (CO or O_2) in 4 nm PtCo nanoparticles and its impact in the turnover frequency of CO oxidation. Similar results were found by Papaefthimiou et al.,[144] who studied the effects of gas phase atmospheres (H_2 or O_2) on the redox behavior of PtCo alloys. As schematized in Figure 14, the distribution of Pt and Co over the first few atomic layers showed that under H_2, Pt is preferentially localized on the surface and Co is in the subsurface region. On the other hand, under O_2, an inverse trend was observed with Co being localized on the surface. A very interesting observation of size dependence was made by

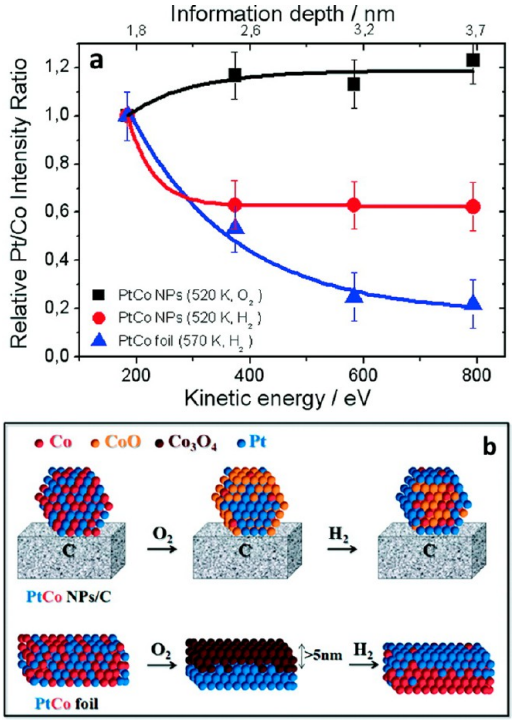

Figure 14. (a) Depth distribution of the Pt/Co atomic ratio obtained by XPS for PtCo nanoparticles in O_2 and in H_2, and for PtCo foil in H_2. (b) Schematic illustration of the evolution of PtCo atom distribution in nanoparticles and foil under O_2 and H_2. Reprinted with permission from ref 144. Copyright 2013, Elsevier.

comparing the behavior of PtCo foil with 3 nm nanoparticles. Under O_2 atmosphere, Co_3O_4 was formed in the foil by oxidation of Co, whereas CoO-like oxide was observed in the nanoparticles. Under H_2, the Co_3O_4 was reduced to metallic Co in the foil, whereas in nanoparticles, a mixture of CoO/Co states was found. Changes in the surface structure according to atmosphere and temperature were also found for NiPt (111) model catalysts by Mu et al.[114]

Bimetallic Ni−Co catalysts applied to SRE and ORE have been studied by our group under SRE[145] and ORE.[146] The results obtained by in situ XANES during H_2-TPR indicated that bimetallic catalysts were more easily reduced than the monometallic ones. In addition, this reducibility of the bimetallic catalysts increased together with the Co content. XANES results measured during ORE indicated that the bimetallic Ni−Co catalysts presented higher resistance to oxidation compared to that of the monometallic catalysts, resulting in a stable catalyst. However, the stability depended on the particle size. Resini et al.[147] showed that during SRE, the formation of CH_4 was lower on Co−Ni supported on YSZ than on the Ni monometallic catalyst. In addition, an increase in H_2 yield was verified at high temperature associated with the steam reforming of CH_4 favored by the alloy formation. Chen et al.[148] observed that the addition of Co to $Ni/Ca\text{-}\gamma\text{-}Al_2O_3$ and Ni/ZrO_2 did not improve the catalytic activity and suggested that the support effect was more important in this case. The support role is discussed in Section 5.

The results described in this section illustrate that the behavior of bimetallic catalysts during SRE and ORE is far from being understood, perhaps because of the difficulty in comparing different studies, and especially the challenges involved in preparing and characterizing supported bimetallic

DOI: 10.1021/cs5020755
ACS Catal. 2015, 5, 3841−3863

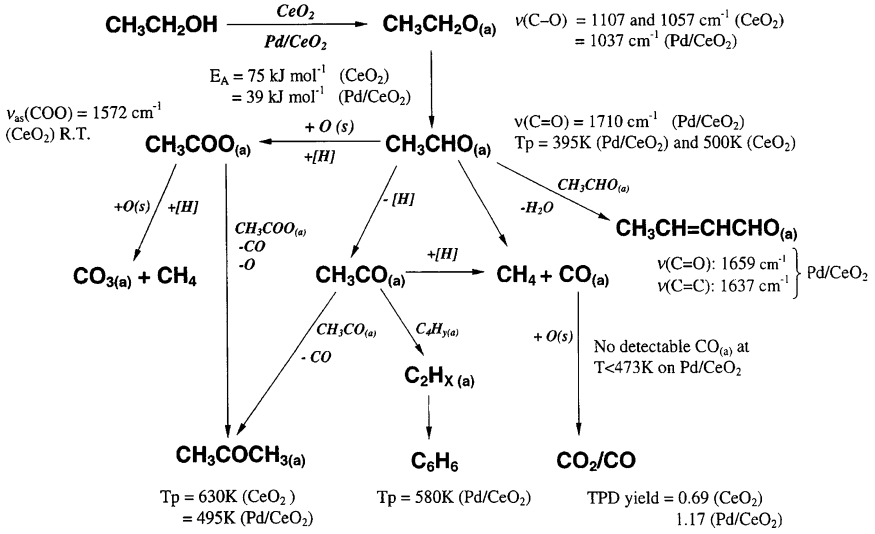

Figure 15. Reaction pathways of ethanol over CeO_2 and Pd/CeO_2. $O_{(s)}$ indicates oxygen from the support. Reprinted with permission from ref 149. Copyright 1999, Elsevier.

catalysts. In addition, the behavior of bimetallic catalysts depends on composition, particle size, and reaction conditions, which vary along the catalytic bed. A thorough characterization of bimetallic catalysts under operando conditions, using techniques such as EXAFS, XANES, XRD, and XPS is crucial for designing and understanding new catalysts for the production of H_2.

5. INFLUENCE OF THE SUPPORT ON THE CATALYST SELECTIVITY AND STABILITY

In the previous sections, we mainly discussed the effect of the metal nanoparticles properties, nature, and structure in the SRE performance. Nevertheless, the support can also play an important role, and several studies have been carried out to identify the ethanol interaction with the metal oxide support and its effect on the activity, selectivity, and stability of SRE catalysts.

5.1. Support Effect on the SRE Reaction Mechanism.

Examples can be found in the literature about ethanol conversion mechanism over metal oxide surfaces. In this aspect, infrared spectroscopy is often used for the identification of the species formed on the support surface, such as ethoxy and acetate species that have been found to be coordinated to different surfaces.[11,14,16,17,149,150]

Several aspects, such as acid–base properties, redox properties, and oxygen mobility, have a strong impact on the role of the support and the metal–support interface on the reaction pathway. In this aspect, ceria[151] is among the most studied supports for SRE catalysts due to its intrinsic activity as a redox catalyst because of the easy reducibility of Ce^{4+} and high mobility of the O^{2-} species within the ceria lattice. Studies of unreduced and reduced ceria, on different crystallographic facets, confirm that both oxidation states and structure deeply affect the adsorption of ethanol, water, intermediaries, and byproducts. In particular, the role of defects and acid–base sites, which are structure-sensitive and also characteristic of several transition metal oxides, is evident in SRE, and opportunities for the design of new catalyst can be foreseen by rational exploration of these properties.[14,152,153]

An early work by Yee at al.[149] compared the species formed when ethanol was exposed on unreduced and reduced polycrystalline ceria. In both cases, ethanol adsorption led to ethoxy formation, but the subsequent formation of acetate species was only observed on unreduced ceria. Therefore, ethanol was oxidized to acetate on the ceria surface but when ceria was reduced, the oxygen/cerium ratio decreased along with its oxidation capability. According to the authors, the acetate formed on the ceria surface was decomposed to carbonate and CH_4 (Figure 15), and the latter could be further reformed to yield hydrogen. In Pd/CeO_2, where the presence of Pd led to a considerable reduction of the ceria support, acetate was not formed, and the aldehyde could be decomposed into carbon monoxide and methane, that underwent reforming, or was dehydrogenated into acetyl (Figure 15). Therefore, in Pd/CeO_2, the acetate formation was inhibited in both reduced and unreduced catalyst, whereas the activity for ethanol dehydrogenation into acetaldehyde increased by 1 order of magnitude compared to neat ceria. Besides acetaldehyde, acetone and benzene were also observed in the product. The absence of ethylene, acetylene, butadiene, and crotonaldehyde suggests that benzene may have been formed through C_2H_x species (from ethoxides) and C_4H_y species (from crotonaldehyde), as observed in Figure 15.

de Lima et al.[154] studied Pt-$CeZrO_2$ catalysts and proposed complex multiple routes for acetate species formation via oxidation of ethoxy or acetaldehyde. In a subsequent publication, the authors found that a fraction of the ethanol can be oxidized to CO and CO_2 instead of forming CH_4.[155] According to Mattos et al.,[14] CH_4 can be formed by different routes from acetate decomposition in the support, while the amount of CH_4 formed in SRE is usually low compared to CO and CO_2 formation.

Mullins et al.[156] studied the interaction of alcohols with $CeO_x(111)$ thin films. Primary alcohols, such as ethanol, adsorbed at low temperature form ethoxy and hydroxyl species. DFT calculations also indicated that ethoxy is the main specie formed on ethanol adsorption on ceria.[157] Formation of acetaldehyde takes place at higher temperature, but on reduced ceria, the O vacancies favored the dehydration reaction through C–O bound breaking that led to ceria oxidation and formation of ethene. Reduced ceria also stabilizes hydroxyls groups, and

DOI: 10.1021/cs5020755
ACS Catal. 2015, 5, 3841–3863

water desorption was hindered.[156] No products originated from C−C breaking or coupling were observed by Mullins et al.[156]

To get more information about the structural dependency on the reactivity of CeO_2, nanoparticles of different shapes (wires, cubes, and octahedra) were analyzed in detail by Li et al.[158] Although wires present a more defective structure, cubes expose {100} facets, and octahedra expose {111} facets. The surface coordinatively unsaturated sites of Ce and O depend on the exposed facet, and the {100} one is the most reactive.[159] However, as pointed out by the authors, acid−base properties, geometry of the adsorption site, reducibility, and oxygen storage capacity are intrinsically related to the exposed crystallographic facet. The reducibility, as mentioned before, affects the dehydrogenation/dehydration selectivities. TPD data of ethanol for all morphologies detected acetaldehyde (dehydrogenation), ethylene (dehydration), and ethanol (desorption) at low temperatures (<250 °C). By increasing the temperature, ethylene was only formed on cubes and wires, and other products such as CO, CO_2, and CH_4 were also detected. The authors described in detail possible reaction pathways for ethanol reaction on ceria surfaces involving deprotonation (forming ethoxy), α-CH scission (desorbing acetaldehyde), β-CH scission (desorbing ethylene), α-CH addition to enolate (desorbing ethylene), acetate formation, and decarboxylation (desorbing CH_4 and CO_2). The different shapes alter the product selectivity by changing the stability of the ethoxy intermediate and the energy barriers to dehydration, dehydrogenation, and decomposition reactions. Similar dependences of the interaction of other molecules such as acetaldehyde,[159−161] CO,[156,162] and H_2O[163−165] on structure and reduction degree of ceria have been reported.[166] Studies under SRE showed that CeO_2 particle morphology[167] and size[168] modify the activity and selectivities of SRE.

Similar examples can be found in the literature about ethanol conversion mechanism over other important oxides surfaces such as Al_2O_3,[169−174] ZnO,[175] MoO_3,[176] ZrO_2,[177] MgO,[178,179] $MgAl_2O_4$, Mg−Al mixed oxides[180,181] and Fe_2O_3.[182] For example, in Al_2O_3, Lewis acidity plays a major role and dehydration (forming ethylene), and etherification (forming diethyl ether) pathways compete; conversely, ethanol dehydrogenation to acetaldehyde is energetically disfavored. Christiansen et al.[172] used DFT calculations to evaluate the ethanol adsorption and reaction over γ-Al_2O_3 (100) and found that diethyl ether and ethylene formation occurs on Lewis acid sites, via Lewis-catalyzed S_N2 and E2 mechanisms, respectively. In both mechanisms, water is formed and competes with ethanol adsorption. DeWilde et al.[171] reported that acetaldehyde can be formed on γ-Al_2O_3 via a shared ethoxy intermediate with the dehydration pathway, through an indirect hydrogen transfer mechanism and formation of ethane. In reducible oxides, dehydrogenation forming acetaldehyde is favored and occurs via cleavage of α-C−H bond of adsorbed ethoxy followed by water formation through Mars and van Krevelen redox mechanism.[158,183] In the case of Mg−Al mixed oxides, the acid−base properties depend on the Mg/Al ratio directly affecting the products rates for ethanol conversion.[181]

It is important to remark that although the support nature and structure may have a clear influence on the ethanol adsorption and reaction pathways, the presence of metal in the supported catalyst may dominate the reaction kinetics. One important parameter is the metal loading, which in the case of noble metal catalyst is typically small (1%), thereby favoring the direct participation of the support on the reaction mechanism. Other parameters that will determine the predominance of metal or support pathways is the type of metal and the reaction conditions.

In the literature, there are many studies on the decomposition of ethanol on different metals and supports, but little is known about the influence of the metal−support interface, which would demonstrate a bifunctional and synergic contribution of different sites in SRE. Zhou et al.[184] showed the impact of metal−oxide interaction on $Ce_{0.8}Ni_{0.2}O_{2-y}$, which modified not only the Ni electronic properties, partially segregated forming nanoparticles under SRE, but also the O vacancy formation, directly affecting the ethanol and H_2O activation. In particular, the production of methane was much smaller in this system. Another example, using Ir/CeO_2 as catalysts, proposed that the reaction mechanism involved the oxidation of ethoxy species to acetate on CeO_2 surface, which then migrated to the Ir surface, where it was decomposed into carbonyl.[185,186] The decomposition of acetate on the metal particle via formation of $*CH_3$ fragment could occur via pyrolitic mechanism. Furthermore, the high oxygen mobility[187] could facilitate the oxygen migration to the metal−support interface, which would favor the oxidation of $*CH_x$ species, suppressing carbon accumulation on the catalyst. However, it is also possible that $*CH_x$ species are oxidized to formaldehyde and carbonate. Although DFT calculations show that the reaction (eq 7) on metal is energetically feasible but kinetically unfavorable, to our knowledge no experimental data have been published that demonstrated the importance of oxidation through a formaldehyde intermediate at the metal−oxide interface. It is desirable that more computational data are generated, addressing kinetics aspects, possible intermediates and spectators, and reaction pathways that would take place at the metal-oxide interface. In this aspect, it is interesting to highlight the significant effort that has been made to understand the mechanism of water-gas shift reaction, and despite the intense debate, the role played by the metal interface in several systems is clear.[188−192] In the case of SRE, one point of common agreement is that the oxygen mobility of the support is a critical property to favor C removal and avoid deactivation.

5.2. Effect of the Support Oxygen Mobility in the Catalyst Performance. The oxygen exchange capacity (oxygen mobility) of the support not only affects the reaction mechanism but also promotes the oxidation of the metal particle and of the adsorbed carbon on catalyst surface.[193,194] For example, it was observed that Co particles are partially oxidized when they are supported on reducible supports, and the presence of both Co^{2+} and Co^0 species leads to an enhancement of the acetaldehyde formation (Figure 16).[195] These results are in good agreement with other works.[14,94,196,197] Stabilization of Co particles in a partially oxidized form allows bifunctional mechanisms, in which oxidative dehydrogenation of ethanol adsorbed on the Co takes place using oxygen supplied by the support.[195] This effect was not observed in nonreducible supports, such as YSZ, due to its low oxygen mobility.[195] However, other works reported an increase in Cu^+ species on Cu nanoparticles when supported on ZrO_2 instead of silica, even though zirconia has low oxygen mobility.[198−200] In this case, the support affects the electronic properties of the metal nanoparticle, changing the Cu^+/Cu ratio, which leads to an increase in the acetaldehyde selectivity from ethanol.

DOI: 10.1021/cs5020755
ACS Catal. 2015, 5, 3841−3863

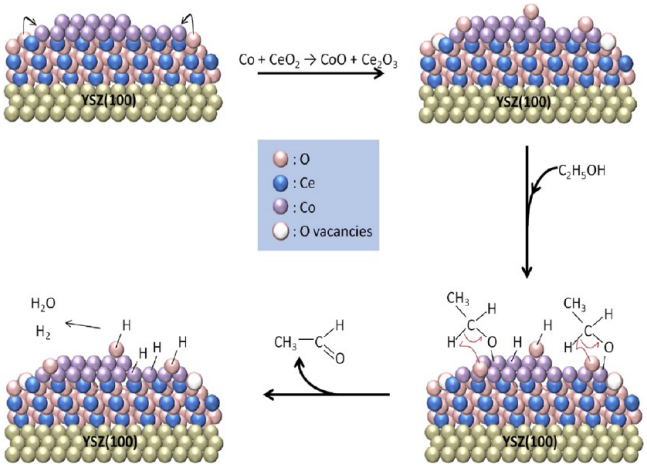

Figure 16. Reaction of ethanol molecules on $Co/CeO_2/YSZ(100)$. Reprinted with permission from ref 195. Copyright 2012, Elsevier.

Song and Ozkan[194] showed that Co/CeO_2 catalyst was more stable under SRE than Co/CeO_2-ZrO_2, or Co/ZrO_2 due to lower carbon accumulation in its surface (Figure 17A–C). As shown in Figure 17D,E, Co/CeO_2 presents a higher oxygen storage capacity and oxygen mobility, allowing a more effective gasification/oxidation of adsorbed carbon on the surface. Studies on Ni/CeO_2 also showed that Ce^{3+} favors the water activation and CO_2 formation.[201] Accordingly, Galetti et al.[202] observed that the modification of $Ni/ZnAl_2O_4$ catalysts with CeO_2 inhibits the accumulation of carbon during SRE at 500 °C with a molar ratio H_2O/ethanol of 4:1. They report that the extent of carbon accumulation depends mainly on the reaction temperature and the Ce/Ni ratio.

The support can also be important to hinder sintering of the metal particles. Comparative studies of the stability of $CeZrO_2$ and $Pt/CeZrO_2$ showed that the Pt-containing catalyst was more selective for hydrogen production; however, it displayed a sharp deactivation in the first 2 h of the reaction (Figure 18).[155] Deactivation by carbon deposition at the metal–support interface rather than by sintering of the Pt (confirmed by TEM) was observed, suggesting a similar effect found in Pt/MgO where graphene sheets nucleated on small Pt nanoparticles and migrate to the support.[111] It was also shown that a simple oxidation–reduction cycle restored the activity of the catalyst because it oxidized the accumulated carbon.[155] The interaction between Pt and ceria was studied by valence photoemission measurements and DFT calculations, revealing a strong metal–support interaction in ultrasmall Pt particles (Pt_8 clusters) that would be responsible for significantly enhance the ability of Pt to adsorb water and dissociate the O–H bonds.[201] This is an interesting result, and several aspects of this interaction can be further analyzed. As previously discussed, the ceria has the ability to partially oxidize the metal nanoparticle, and therefore, the interaction between Pt and ceria could take place through PtO_x sites, which has been reported to be stronger than interaction through Pt^0.[203] Furthermore, metal–support interaction has also been observed under SRE conditions in other catalysts based on nonreducible supports, such as Co/SiO_2,[204] and Ni/ZrO_2.[205] These results endorse the argument that the metal particle electronic properties could be affected by the support independent of the oxygen mobility.

5.3. Reactivity of Ethanol in ORE. ORE reaction has been studied on supported metal catalysts aiming to achieve higher stability against carbon deposition. In general, the oxygen addition to the feed decreases the carbon accumulation on the catalyst, but it decreases the hydrogen yield by undesired reactions, such as the ethanol overoxidation to CO and CO_2.

Several studies have been carried out to understand the role of the support for ORE reaction. As in other systems, increasing

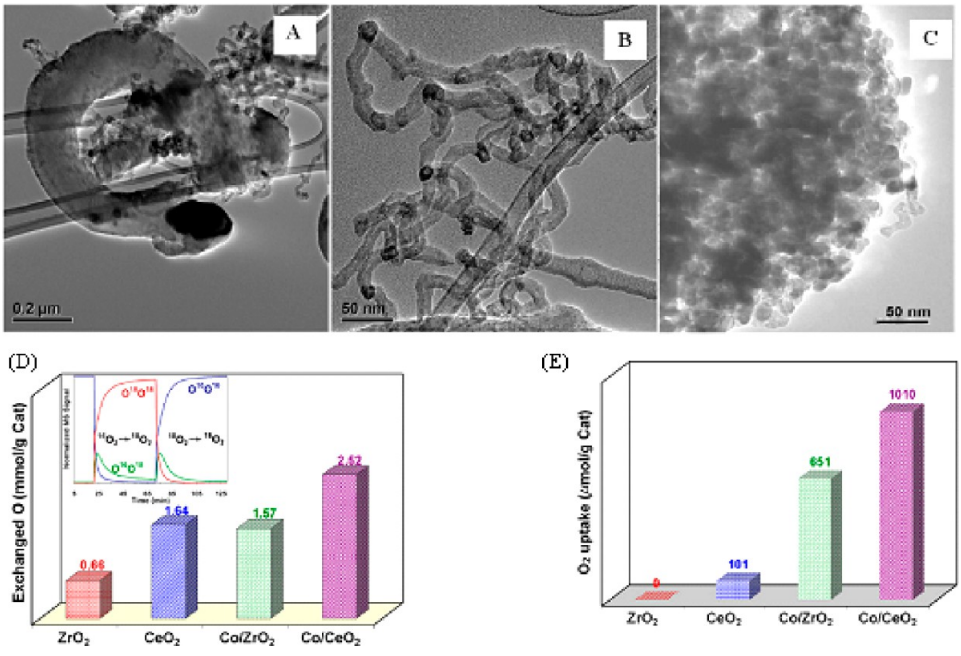

Figure 17. TEM images of Co supported catalysts after SRE at 450 °C using ethanol/H_2O molar ratio of 1:10. (A) and (B) $10\%Co/ZrO_2$, (C) $10\%Co/10\%CeO_2$–ZrO_2. (D) Oxygen exchange measured using $^{16}O_2/^{18}O_2$ switch over ceria and zirconia supports and corresponding Co supported catalysts; (E) Oxygen uptake during O_2 pulse chemisorption of the same supports and catalysts. Adapted with permission from ref 194. Copyright 2009, Elsevier.

DOI: 10.1021/cs5020755
ACS Catal. 2015, 5, 3841–3863

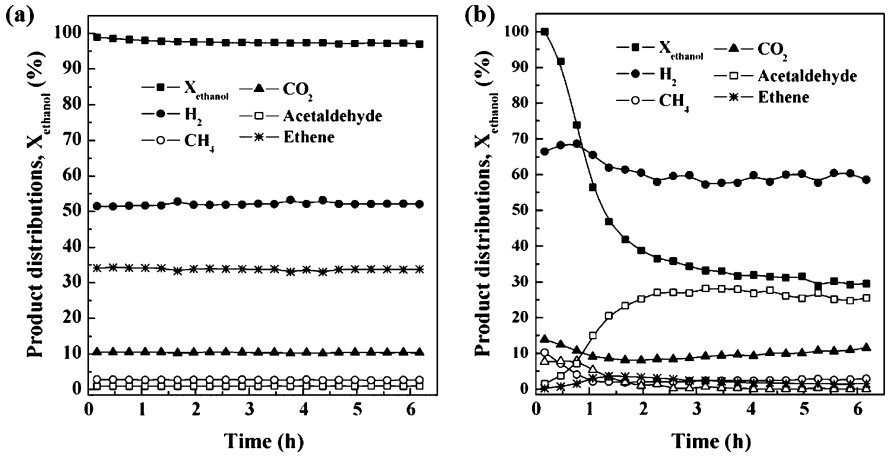

Figure 18. Ethanol conversion ($X_{ethanol}$) and product distributions during SRE at 773 K with ethanol/H_2O molar ratio of 1:3 on (a) $CeZrO_2$ and (b) Pt/$CeZrO_2$. Reprinted with permission from ref 155. Copyright 2009, Elsevier.

the surface area of the support contributes to better metal dispersion and improves the catalytic activity.[206,207]

Cai et al.[186] studied Ir/CeO_2 catalysts and showed dependence of ORE on the support morphology and structure. Lower support calcination temperatures (400 or 550 °C) led to more stable catalysts compare to higher calcination temperature (700 or 850 °C), as shown in Figure 19. According to the

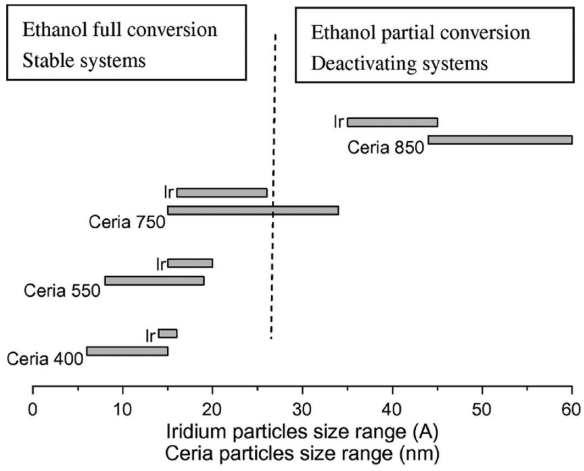

Figure 19. Impact on Ir and ceria particle sizes after catalyst aging under ORE at 650 °C for 60 h (initial to final values for each bar: from left- to right-hand side). Reprinted with permission from ref 186. Copyright 2012, Elsevier.

authors, the correlation of stability with temperature of calcination was due to strong basicity and high concentration of surface defects achieved by calcining at lower temperature, which increased the metal–support interaction, facilitated the oxygen activation and diffusion, and inhibited the carbon deposition. The deactivation of the catalysts prepared with ceria previously calcined at 700 or 850 °C was attributed to carbon accumulation and sintering of both Ir and CeO_2 particles.

Concerning the nature of the support, Avila-Neto et al.[13] compared the performance of La_2O_3–Al_2O_3 and CeO_2–Al_2O_3 support with the corresponding Co supported catalysts in ORE at 773 K (Figure 20). La_2O_3–Al_2O_3 presented poor activity to ethanol conversion, and the predominant product was acetaldehyde (Figure 20a). CeO_2–Al_2O_3 was more active to ethanol conversion, and the main products were CO and CO_2 (Figure 20c), obtained by the overoxidation of ethanol due to the high oxygen mobility of ceria. For both supports, low selectivity for H_2 and CH_4 were obtained. Addition of Co to the supports greatly increased the H_2 formation (Figure 20b,c), and both catalysts presented comparable performances. The slightly greater formation of CO and CO_2 on CeO_2–Al_2O_3 was assigned to oxidation of ethanol over ceria.[206]

5.4. Influence of the Support Acid–Base Properties in SRE and ORE. Acid–base properties of the supports can be tailored by changing their composition, which has shown to affect the catalyst performance in SRE and ORE.[193,208,209] In fact, one of the main concerns on designing catalysts for SRE and ORE is to reduce the yields of the byproducts, and it is important to understand the reaction route that maximizes selectivity to H_2. For example, the dehydration of ethanol to diethyl ether and/or ethylene (eqs 14,15) can take place on acidic/basic supports.[210] As previously mentioned, over alumina, the reaction requires strong Lewis acid.[169–174,211] Over zeolites, the ethanol dehydration is determined by the stability of intermediates, by the size of the zeolite channels, and by the position of Brønsted acid sites.[212] Over basic solids, such as MgO, the dehydration involves strong basic sites and weak Lewis acid sites, which catalyze both dehydration to ethylene and dehydrogenation to acetaldehyde.[178,179,213] The formation of ethylene is particularly undesirable since it promotes secondary reactions, such as oligomerization and coke formation.

$$2CH_3{-}CH_2{-}OH \leftrightarrows CH_3{-}CH_2{-}O{-}CH_2{-}CH_3 + H_2O \quad (14)$$

$$CH_3{-}CH_2{-}OH \leftrightarrows H_2C{=}CH_2 + H_2O \quad (15)$$

Dehydrogenation of ethanol to acetaldehyde (eq 3) is favored at low temperatures and takes place over both metals and oxides. The formed acetaldehyde can also undergo condensation reactions over acidic and basic oxides to form an aldol, which can be further dehydrated to crotonaldehyde by an acid site.[214,215] In general, the acidity favors condensation reactions with polymerization to heavy products.

Depending on the nature of the support, acetone can be formed under SRE by a complex reaction route involving: (i) acetaldehyde oxidation; (ii) coupling with an acetate molecule; and (iii) decarboxylation. Acetone can also be formed by condensation of acetaldehyde followed by oxidation of aldol product, which is then dehydrogenated and decarboxy-

DOI: 10.1021/cs5020755
ACS Catal. 2015, 5, 3841–3863

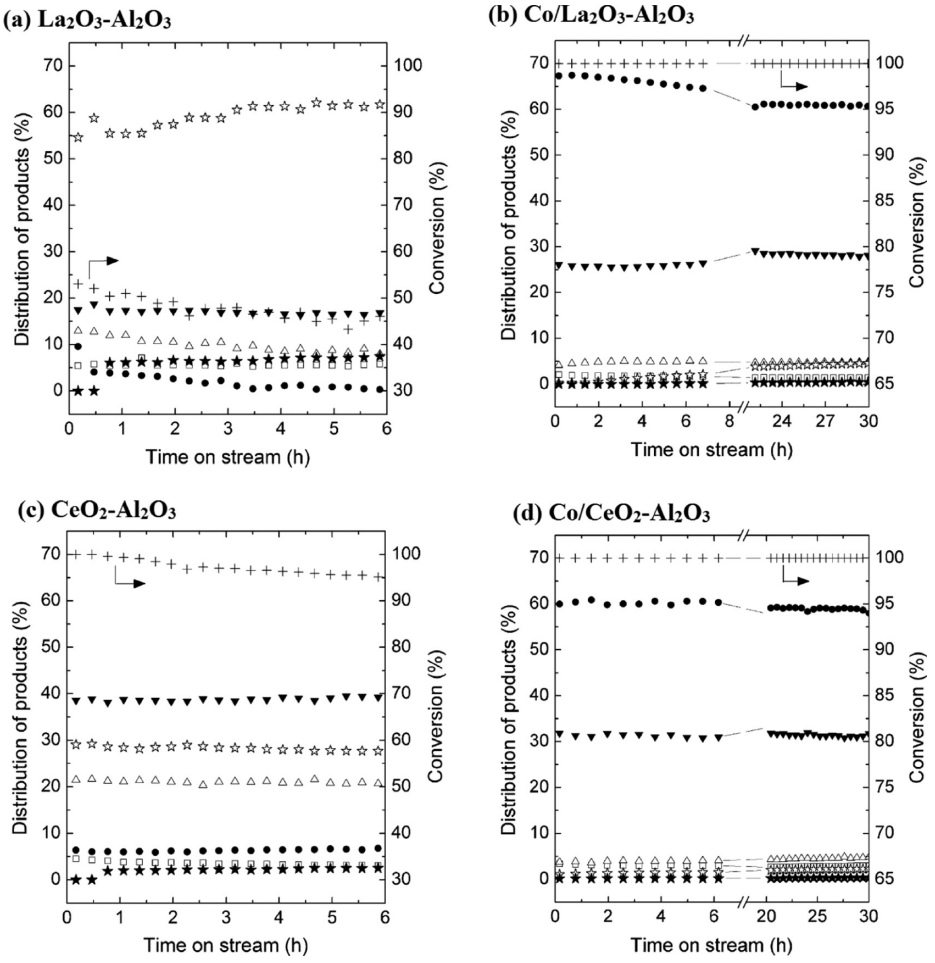

Figure 20. Ethanol conversion and products distribution for ORE on (a) La_2O_3−Al_2O_3 and (c) CeO_2−Al_2O_3 supports and corresponding Co-supported catalysts ((b) and (d), respectively) at 773 K and H_2O/ethanol/O_2 molar composition of 3:1:0.5: (+) ethanol conversion, (●) H_2, (□) CH_4, (Δ) CO, (▼) CO_2, (★) ethylene and (☆) acetaldehyde. Reprinted with permission from ref 13. Copyright 2012, Elsevier.

lated.[197,216−220] In both pathways, oxygen for the oxidation steps can be provided by water activation or by the support, on reducible oxides. A high selectivity to acetone was observed on catalysts containing both acidic and basic sites as well as redox properties, such as Fe_2O_3, ZnO, and V_2O_5.[182,183,219]

The support acid−base properties can also affect the metal particle size, which consequently affects the catalytic performance and stability. Youn et al.[221] studied the effect of support acidity on ORE by using Ni supported on different oxides: ZnO, MgO, ZrO_2, TiO_2, and Al_2O_3, finding a correlation (volcano plot) between H_2 yield and support acidity. Other reports showed that catalyst performance and stability under SRE were also affected by the modification of the support with alkali metals. For example, the addition of 1% of Na^+, Li^+, or K^+ on Ni/MgO inhibited Ni sintering; however, it did not prevent carbon formation.[222,223] Addition of Na^+ to Co/ZnO increased slightly the catalytic activity and decreased the deactivation by carbon deposition.[224] Domok et al.[225] observed that SRE activity and selectivity to H_2 were increased when K^+ was used as promoter on 1% Pt/Al_2O_3. The effects of K^+ loading on Rh/CeO_2−ZrO_2 catalysts with various CeO_2/ZrO_2 ratios on SRE were also observed by Roh et al.[226]

Alkaline earth metals (Mg, Ca) have also been used to modify supported metal catalysts for both SRE and ORE. For example, Choong et al.[227] investigated the effect of Ca^{2+} on Ni/Al_2O_3 catalysts for SRE at low temperatures and found that the Al_2O_3 acidity was reduced by Ca^{2+} addition, reducing ethanol dehydration and ethylene formation. Furthermore, Ca^{2+} led to an increase in water adsorption, resulting in high ethanol conversion to H_2, CH_4, and CO_2. Similar results[138] were also reported for Ca^{2+} doped Ni/CeO_2−ZrO_2 at low reaction temperature (400−550 °C). Carrero et al.[135] observed an improvement on H_2 production and lower carbon accumulation for SRE at 600 °C in Cu−Ni supported on Mg^{2+} or Ca^{2+}-modified silica. This effect could be related to better dispersion of Cu−Ni caused by dopant, through stronger metal−support interactions. Song and Ozkan[228] observed an increase in the oxygen mobility on ceria doped with Ca^{2+}, with a positive impact for SRE. Contrarily, Granados et al.[229] reported that the addition of Ca^{2+} into $CeZrO_4$ support led to a decrease in the oxygen storage capacity.

6. CONCLUDING REMARKS AND OPPORTUNITIES

SRE/ORE should become important reactions for H_2 production at industrial scale in the future. For large-scale applications, more abundant metals such as Ni and Co are more attractive than noble metals, but integrated portable technologies have a different set of constraints that may only be achieved with other classes of catalysts. In both cases, there are still key steps to be overcome to understand the catalyst behavior during SRE or ORE and optimize its performance. In this aspect, both theoretical studies and experimental

DOI: 10.1021/cs5020755
ACS Catal. 2015, 5, 3841−3863

investigations have to be pursued together. The availability of operando characterization tools is a great opportunity to a deeper understanding of the several parameters that affect the catalyst performance. Therefore, a better understanding of the fundamental aspects of ethanol reforming should lead toward the development of new high performance catalysts.

We suggest that three key aspects should be clarified to allow a better understanding of the ethanol reforming reaction: (i) the effect of the metal nature—impact of particle size and metal oxidation state in the SRE performance; (ii) the importance of metal surface electronic properties to obtain a balanced and stable catalyst; and (iii) the influence of the support on the catalyst selectivity and stability. The knowledge of the reaction mechanism is fundamental for analyzing the experimental data related to the three aspects mentioned.

As discussed, ethanol activation pathways depend on the metal nature and can be generally divided in two groups: the less-oxophilic metals (Pd and Pt), in which α-C-H activation takes place, and the more-oxophilic metals (Co, Ni, Rh, Ru), which promote activation via O−H. An increase in the temperature favors the H abstraction, going through the formation of intermediates such as CH_3C^*O, $^*CH_2C^*O$, and $^*CHC^*O$. The cleavage of C−C bond is expected to be favored in species highly dehydrogenated. After the cleavage of C−C bond, $^*CH_x$ and *CO species are formed, and finally, the $^*CH_x$ species are decomposed, forming *C that has to be oxidized to CO. The CH_4 selectivity at low temperature is governed by the ability of the metal to hydrogenate/dehydrogenate the $^*CH_x$ species, which is favored in highly reduced metals such as Ni. An increase of metal surface reactivity is expected from Pt to Co, favoring H abstraction and increasing the availability of O* on the metal surface and disfavoring hydrogenation reactions at low temperatures.

Among the several parameters that rule the catalyst performance, it is clear that metal particle size plays a major role, and it is intrinsically related to important aspects of the catalysts, such as resistance to carbon deposition and stability of the metallic phase against oxidation. Metal particle size will also enhance interface effects, and the optimum metal particle size will depend on the metal nature, support type, and reaction conditions. In particular, the optimum size range should be different for SRE and ORE; the presence of O_2 in ORE and the higher tendency of small particles to be oxidized will shift the ideal size to larger values compared to SRE. Finally, due to the variation of the redox potential of the reaction atmosphere along the reaction bed, both opportunities and challenges can be foreseen in practical applications.

Related to the support, aspects such as oxygen storage capacity/oxygen mobility affect the reaction mechanism, but experimental and theoretical data are still far from elucidating the influence of support as well as metal−support interface, in particular in the case of oxidation and hydrogenation of C*, CH_x*, and other species. The experimental results point out that in SRE, reducible supports seem to be a better option because they increase resistance to carbon accumulation. However, in ORE, the oxygen is added to the feed, and the support may play a different role. The nature of the support affects other important parameters, such as acidity and basicity affecting the formation of byproducts. Because the support also affects metal particle stability against sintering, deeper studies about the deactivation mechanism under SRE and ORE are desired.

Co- and Ni-based catalysts are cheaper and probably the most promising catalytically active metals for industrial SRE. However, the catalytic properties should be improved; for example, Co is very reactive toward oxygen, and the stability of the Co−CoO system is still uncertain. In the case of Ni, which shows lower reactivity toward oxygen, it shows high hydrogenation activity, with significant formation of CH_4 at low temperatures. Metal surfaces showing high reactivity toward oxygen at low temperature are easily oxidized by H_2O and become active mainly to ethanol oxidation, forming acetaldehyde. Contrarily, a metal surface with low reactivity to oxygen enhances the activity of hydrogenation of the intermediates, favoring CH_4 formation. This reactivity with oxygen is correlated with catalyst deactivation due to carbon accumulation, metal oxidation, and metal sintering (metal−support interaction). The balance to achieve a good performance involves fine-tuning of electronic properties through alloy formation, metal particle size, and nature of support. These are challenging issues that need to be solved to enable the successful design of new and stable catalysts. With the advances in theoretical and experimental tools, exciting results can be foreseen in the near future.

AUTHOR INFORMATION

Corresponding Author

*E-mail: jmcb@ufscar.br.

Notes

The authors declare no competing financial interest.

ACKNOWLEDGMENTS

The authors are grateful for the financial support of FAPESP, Project No. 2011/50727-9 (Fundação de Amparo à Pesquisa do Estado de São Paulo), CNPq (Conselho Nacional de Desenvolvimento Científico e Tecnológico), Project FNI E02/16, and Brazilian Synchrotron Light Laboratory (LNLS). The authors gratefully acknowledge their students and co-workers that have contributed with fruitful discussion over the years.

REFERENCES

(1) Bridger, G. W.; Kemball, C.; Dowden, D. A. The steam reforming of hydrocarbons. In *Catalysis*; Kemball, C., Dowden, D. A., Eds.; The Royal Society of Chemistry: London, 1980; Vol. 3, pp 39−69.

(2) Rostrup-Nielsen, J. R. Catalytic steam reforming. In *Catalysis-Science & Technology*; Anderson, J. R., Boudart, M., Eds.; Springer-Verlag: Berlin, 1984; Vol. 5, pp 3−110.

(3) Inui, T.; Spivey, J. J. Reforming of CH_4 by CO_2, O_2 and/or H_2O. In *Catalysis*; Spivey, J. J., Ed.; The Royal Society of Chemistry: London, 2002; Vol. *16*, pp 133−154.

(4) Bion, N.; Epron, F.; Duprez, D. Bioethanol reforming for H_2 production. A comparison with hydrocarbon reforming. In *Catalysis*; Spivey, J. J., Dooley, K. M., Eds.; The Royal Society of Chemistry: London, 2010; Vol. *22*, pp 1−55.

(5) Besenbacher, F.; Chorkendorff, I.; Clausen, B. S.; Hammer, B.; Molenbroek, A. M.; Norskov, J. K.; Stensgaard, I. *Science* **1998**, *279*, 1913−1915.

(6) Liberatori, J. W. C.; Ribeiro, R. U.; Zanchet, D.; Noronha, F. B.; Bueno, J. M. C. *Appl. Catal., A* **2007**, *327*, 197−204.

(7) Sinfelt, J. H.; Yates, D. J. C. *J. Catal.* **1967**, *8*, 82−90.

(8) Somorjai, G. A. *Introduction to Surface Chemistry and Catalysis*; Wiley: New York, 1994.

(9) Bion, N.; Duprez, D.; Epron, F. *ChemSusChem* **2012**, *5*, 76−84.

(10) Aupretre, F.; Descorme, C.; Duprez, D. *Catal. Commun.* **2002**, *3*, 263−267.

(11) Frusteri, F.; Freni, S.; Spadaro, L.; Chiodo, V.; Bonura, G.; Donato, S.; Cavallaro, S. *Catal. Commun.* **2004**, *5*, 611−615.

DOI: 10.1021/cs5020755
ACS Catal. 2015, 5, 3841−3863

(12) Karim, A. M.; Su, Y.; Sun, J.; Yang, C.; Strohm, J. J.; King, D. L.; Wang, Y. *Appl. Catal., B* **2010**, *96*, 441−448.
(13) Avila-Neto, C. N.; Liberatori, J. W. C.; da Silva, A. M.; Zanchet, D.; Hori, C. E.; Noronha, F. B.; Bueno, J. M. C. *J. Catal.* **2012**, *287*, 124−137.
(14) Mattos, L. V.; Jacobs, G.; Davis, B. H.; Noronha, F. b. B. *Chem. Rev.* **2012**, *112*, 4094−4123.
(15) de la Piscina, P. R.; Homs, N. Ethanol Reformation to Hydrogen. In *Alcoholic Fuels*; Minteer, S., Ed.; CRC Press: Boca Raton, FL, 2006; pp 233−248.
(16) de la Piscina, P. R.; Homs, N. *Chem. Soc. Rev.* **2008**, *37*, 2459−2467.
(17) Haryanto, A.; Fernando, S.; Murali, N.; Adhikari, S. *Energy Fuels* **2005**, *19*, 2098−2106.
(18) James, O. O.; Maity, S.; Mesubi, M. A.; Ogunniran, K. O.; Siyanbola, T. O.; Sahu, S.; Chaubey, R. *Green Chem.* **2011**, *13*, 2272−2284.
(19) Bligaard, T.; Norskov, J. K. Heterogeneous catalysis. In *Chemical Bonding at Surfaces and Interfaces*; Nilsson, A., Pettersson, L. G. M., Norskov, J. K., Eds.; Elsevier: Amsterdam, 2008; pp 255−321.
(20) Gates, S. M.; Russell, J. N., Jr; Yates, J. T., Jr *Surf. Sci.* **1986**, *171*, 111−134.
(21) Fatsikostas, A. N.; Verykios, X. E. *J. Catal.* **2004**, *225*, 439−452.
(22) Song, H.; Zhang, L.; Ozkan, U. S. *Ind. Eng. Chem. Res.* **2010**, *49*, 8984−8989.
(23) Sahoo, D. R.; Vajpai, S.; Patel, S.; Pant, K. K. *Chem. Eng. J.* **2007**, *125*, 139−147.
(24) Ribeiro, R. U.; Liberatori, J. W. C.; Winnishofer, H.; Bueno, J. M. C.; Zanchet, D. *Appl. Catal., B* **2009**, *91*, 670−678.
(25) Jones, G.; Jakobsen, J. G.; Shim, S. S.; Kleis, J.; Andersson, M. P.; Rossmeisl, J.; Abild-Pedersen, F.; Bligaard, T.; Helveg, S.; Hinnemann, B.; Rostrup-Nielsen, J. R.; Chorkendorff, I.; Sehested, J.; Norskov, J. K. *J. Catal.* **2008**, *259*, 147−160.
(26) Watwe, R. M.; Bengaard, H. S.; Rostrup-Nielsen, J. R.; Dumesic, J. A.; Norskov, J. K. *J. Catal.* **2000**, *189*, 16−30.
(27) Bengaard, H. S.; Norskov, J. K.; Sehested, J.; Clausen, B. S.; Nielsen, L. P.; Molenbroek, A. M.; Rostrup-Nielsen, J. R. *J. Catal.* **2002**, *209*, 365−384.
(28) Alcalá, R.; Mavrikakis, M.; Dumesic, J. A. *J. Catal.* **2003**, *218*, 178−190.
(29) Lee, A. F.; Gawthrope, D. E.; Hart, N. J.; Wilson, K. *Surf. Sci.* **2004**, *548*, 200−208.
(30) Weststrate, C. J.; Ludwig, W.; Bakker, J. W.; Gluhoi, A. C.; Nieuwenhuys, B. E. *ChemPhysChem* **2007**, *8*, 932−937.
(31) Skoplyak, O.; Barteau, M. A.; Chen, J. G. *Surf. Sci.* **2008**, *602*, 3578−3587.
(32) Sutton, J. E.; Panagiotopouou, P.; Veryldos, X. E.; Vlachos, D. G. *J. Phys. Chem. C* **2013**, *117*, 4691−4706.
(33) Cong, Y.; van Spaendonk, V.; Masel, R. I. *Surf. Sci.* **1997**, *385*, 246−258.
(34) Ma, Y.; Hernandez, L.; Guadarrama-Perez, C.; Balbuena, P. B. *J. Phys. Chem. A* **2012**, *116*, 1409−1416.
(35) Davis, J. L.; Barteau, M. A. *Surf. Sci.* **1987**, *187*, 387−406.
(36) Davis, J. L.; Barteau, M. A. *Surf. Sci.* **1988**, *197*, 123−152.
(37) Davis, J. L.; Barteau, M. A. *Surf. Sci.* **1990**, *235*, 235−248.
(38) Shekhar, R.; Barteau, M. *Catal. Lett.* **1995**, *31*, 221−237.
(39) Williams, R. M.; Pang, S. H.; Medlin, J. W. *Surf. Sci.* **2014**, *619*, 114−118.
(40) Li, M.; Guo, W. Y.; Jiang, R. B.; Zhao, L. M.; Shan, H. H. *Langmuir* **2010**, *26*, 1879−1888.
(41) Sutton, J. E.; Vlachos, D. G. Ethanol activation on closed-packed surfaces. *Ind. Eng. Chem. Res.* DOI: 10.1021/ie5043374.
(42) Wang, J. H.; Lee, C. S.; Lin, M. C. *J. Phys. Chem. C* **2009**, *113*, 6681−6688.
(43) Houtman, C. J.; Barteau, M. A. *J. Catal.* **1991**, *130*, 528−546.
(44) Sturm, J. M.; Lee, C. J.; Bijkerk, F. *Surf. Sci.* **2013**, *612*, 42−47.
(45) Brown, N. F.; Barteau, M. A. *Langmuir* **1995**, *11*, 1184−1189.
(46) Li, M.; Guo, W.; Jiang, R.; Zhao, L.; Lu, X.; Zhu, H.; Fu, D.; Shan, H. *J. Phys. Chem. C* **2010**, *114*, 21493−21503.
(47) Choi, Y.; Liu, P. *Catal. Today* **2011**, *165*, 64−70.
(48) Sheng, P. Y.; Yee, A.; Bowmaker, G. A.; Idriss, H. *J. Catal.* **2002**, *208*, 393−403.
(49) Resta, A.; Gustafson, J.; Westerstrom, R.; Mikkelsen, A.; Lundgren, E.; Andersen, J. N.; Yang, M.-M.; Ma, X.-F.; Bao, X.-H.; Li, W.-X. *Surf. Sci.* **2008**, *602*, 3057−3063.
(50) Zhang, J.; Zhong, Z. Y.; Cao, X. M.; Hu, P.; Sullivan, M. B.; Chen, L. W. *ACS Catal.* **2014**, *4*, 448−456.
(51) Kasza, R. V.; Griffiths, K.; Shapter, J. G.; Norton, P. R.; Harrington, D. A. *Surf. Sci.* **1996**, *356*, 195−208.
(52) Michaelides, A.; Hu, P. *J. Chem. Phys.* **2000**, *112*, 6006−6014.
(53) Kandoi, S.; Gokhale, A. A.; Grabow, L. C.; Dumesic, J. A.; Mavrikakis, M. *Catal. Lett.* **2004**, *93*, 93−100.
(54) Cao, Y. L.; Chen, Z. X. *Surf. Sci.* **2006**, *600*, 4572−4583.
(55) Wang, G. C.; Tao, S. X.; Bu, X. H. *J. Catal.* **2006**, *244*, 10−16.
(56) Pozzo, M.; Carlini, G.; Rosei, R.; Alfe, D. *J. Chem. Phys.* **2007**, *126*, 164706.
(57) Grabow, L. C.; Gokhale, A. A.; Evans, S. T.; Dumesic, J. A.; Mavrikakis, M. *J. Phys. Chem. C* **2008**, *112*, 4608−4617.
(58) Phatak, A. A.; Delgass, W. N.; Ribeiro, F. H.; Schneider, W. F. *J. Phys. Chem. C* **2009**, *113*, 7269−7276.
(59) Ratnasamy, C.; Wagner, J. P. *Catal. Rev.: Sci. Eng.* **2009**, *51*, 325−440.
(60) Rhodes, C.; Hutchings, G. J.; Ward, A. M. *Catal. Today* **1995**, *23*, 43−58.
(61) Palo, D. R.; Dagle, R. A.; Holladay, J. D. *Chem. Rev.* **2007**, *107*, 3992−4021.
(62) Lin, S.; Xie, D.; Guo, H. *J. Phys. Chem. C* **2011**, *115*, 20583−20589.
(63) Yuan, Y.; Yan, N.; Dyson, P. J. *ACS Catal.* **2012**, *2*, 1057−1069.
(64) Christensen, K. O.; Chen, D.; Lodeng, R.; Holmen, A. *Appl. Catal., A* **2006**, *314*, 9−22.
(65) Navrotsky, A.; Ma, C.; Lilova, K.; Birkner, N. *Science* **2010**, *330*, 199−201.
(66) Song, H.; Mirkelamoglu, B.; Ozkan, U. S. *Appl. Catal., A* **2010**, *382*, 58−64.
(67) Vizcaino, A. J.; Carrero, A.; Calles, J. A. *Int. J. Hydrogen Energy* **2007**, *32*, 1450−1461.
(68) Bussi, J.; Bespalko, N.; Veiga, S.; Amaya, A.; Faccio, R.; Abello, M. C. *Catal. Commun.* **2008**, *10*, 33−38.
(69) Romero, A.; Jobbágy, M.; Laborde, M.; Baronetti, G.; Amadeo, N. *Catal. Today* **2010**, *149*, 407−412.
(70) Kugai, J.; Subramani, V.; Song, C. S.; Engelhard, M. H.; Chin, Y. H. *J. Catal.* **2006**, *238*, 430−440.
(71) Guil-López, R.; Navarro, R. M.; Penã, M. A.; Fierro, J. L. G. *Int. J. Hydrogen Energy* **2011**, *36*, 1512−1523.
(72) Li, M.; Wang, X.; Li, S.; Wang, S.; Ma, X. *Int. J. Hydrogen Energy* **2010**, *35*, 6699−6708.
(73) Liu, J.-Y.; Lee, C.-C.; Wang, C.-H.; Yeh, C.-T.; Wang, C.-B. *Int. J. Hydrogen Energy* **2010**, *35*, 4069−4075.
(74) Chen, H. Q.; Yu, H.; Peng, F.; Yang, G. X.; Wang, H. J.; Yang, J.; Tang, Y. *Chem. Eng. J.* **2010**, *160*, 333−339.
(75) Wu, C.; Williams, P. T. *Environ. Sci. Technol.* **2010**, *44*, 5993−5998.
(76) de Lima, S. M.; da Silva, A. M.; da Costa, L. O. O.; Assaf, J. M.; Jacobs, G.; Davis, B. H.; Mattos, L. V.; Noronha, F. b. B. *Appl. Catal., A* **2010**, *377*, 181−190.
(77) Valderrama, G.; Goldwasser, M. R.; Navarro, C. U.; Tatibouet, J. M.; Barrault, J.; Batiot-Dupeyrat, C.; Martínez, F. *Catal. Today* **2005**, *107−108*, 785−791.
(78) Penã, M. A.; Fierro, J. L. G. *Chem. Rev.* **2001**, *101*, 1981−2018.
(79) He, L.; Berntsen, H.; Ochoa-Fernandez, E.; Walmsley, J.; Blekkan, E.; Chen, D. *Top. Catal.* **2009**, *52*, 206−217.
(80) da Silva, A. L. M.; den Breejen, J. P.; Mattos, L. V.; Bitter, J. H.; de Jong, K. P.; Noronha, F. B. *J. Catal.* **2014**, *318*, 67−74.
(81) van Steen, E.; Claeys, M.; Dry, M. E.; van de Loosdrecht, J.; Viljoen, E. L.; Visagie, J. L. *J. Phys. Chem. B* **2005**, *109*, 3575−3577.
(82) Luo, W.; Asthagiri, A. *Catal. Sci. Technol.* **2014**, *4*, 3379−3389.

DOI: 10.1021/cs5020755
ACS Catal. 2015, 5, 3841−3863

(83) Zheng, F.; Alayoglu, S.; Guo, J.; Pushkarev, V.; Li, Y.; Glans, P.-A.; Chen, J.-l.; Somorjai, G. *Nano Lett.* **2011**, *11*, 847−853.
(84) Frusteri, F.; Freni, S.; Chiodo, V.; Donato, S.; Bonura, G.; Cavallaro, S. *Int. J. Hydrogen Energy* **2006**, *31*, 2193−2199.
(85) Pereira, E. B.; Homs, N.; Marti, S.; Fierro, J. L. G.; de la Piscina, P. R. *J. Catal.* **2008**, *257*, 206−214.
(86) da Silva, A. L. M.; Mattos, L. V.; den Breejen, J. P.; Bitter, J. H.; de Jong, K. P.; Noronha, F. B. *Catal. Today* **2011**, *164*, 262−267.
(87) Potoczna-Petru, D.; Kepinski, L. *Catal. Lett.* **2001**, *73*, 41−46.
(88) Nam, K. M.; Shim, J. H.; Han, D. W.; Kwon, H. S.; Kang, Y. M.; Li, Y.; Song, H.; Seo, W. S.; Park, J. T. *Chem. Mater.* **2010**, *22*, 4446−4454.
(89) Papaefthimiou, V.; Dintzer, T.; Dupuis, V.; Tamion, A.; Tournus, F.; Hillion, A.; Teschner, D.; Havecker, M.; Knop-Gericke, A.; Schlogl, R.; Zafeiratos, S. *ACS Nano* **2011**, *5*, 2182−2190.
(90) Zonnevylle, M. C.; Geerlings, J. J. C.; van Santen, R. A. *Surf. Sci.* **1990**, *240*, 253−262.
(91) Herranz, T.; Deng, X.; Cabot, A.; Guo, J.; Salmeron, M. *J. Phys. Chem. B* **2009**, *113*, 10721−10727.
(92) Banares, M. A. *Catal. Today* **2005**, *100*, 71−77.
(93) Topsoe, H. *J. Catal.* **2003**, *216*, 155−164.
(94) Martono, E.; Vohs, J. M. *ACS Catal.* **2011**, *1*, 1414−1420.
(95) Llorca, J.; Dalmon, J. A.; de la Piscina, P. R.; Homs, N. *Appl. Catal., A* **2003**, *243*, 261−269.
(96) de la Peña O'Shea, V. A.; Homs, N.; Pereira, E. B.; Nafria, R.; de la Piscina, P. R. *Catal. Today* **2007**, *126*, 148−152.
(97) Karim, A. M.; Su, Y.; Engelhard, M. H.; King, D. L.; Wang, Y. *ACS Catal.* **2011**, *1*, 279−286.
(98) Lebarbier, V. M.; Karim, A. M.; Engelhard, M. H.; Wu, Y.; Xu, B. Q.; Petersen, E. J.; Datye, A. K.; Wang, Y. *ChemSusChem* **2011**, *4*, 1679−1684.
(99) Xu, J.; Saeys, M. *J. Catal.* **2006**, *242*, 217−226.
(100) Nieskens, D. L. S.; Jansen, M. M. M.; van Bavel, A. P.; Curulla-Ferre, D.; Niemantsverdriet, J. W. *Phys. Chem. Chem. Phys.* **2006**, *8*, 624−632.
(101) Llobet, S.; Pinilla, J. L.; Moliner, R.; Suelves, I. *Fuel* **2015**, *139*, 71−78.
(102) Sharma, R.; Moore, E.; Rez, P.; Treacy, M. M. J. *Nano Lett.* **2009**, *9*, 689−694.
(103) Lin, M.; Ying Tan, J. P.; Boothroyd, C.; Loh, K. P.; Tok, E. S.; Foo, Y. L. *Nano Lett.* **2006**, *6*, 449−452.
(104) Hofmann, S.; Sharma, R.; Ducati, C.; Du, G.; Mattevi, C.; Cepek, C.; Cantoro, M.; Pisana, S.; Parvez, A.; Cervantes-Sodi, F.; Ferrari, A. C.; Dunin-Borkowski, R.; Lizzit, S.; Petaccia, L.; Goldoni, A.; Robertson, J. *Nano Lett.* **2007**, *7*, 602−608.
(105) Bell, A. T. *Nature* **2008**, *456*, 185−186.
(106) Baker, R. T. K.; Harris, P. S.; Thomas, R. B.; Waite, R. J. *J. Catal.* **1973**, *30*, 86−95.
(107) Rodriguez-Manzo, J. A.; Terrones, M.; Terrones, H.; Kroto, H. W.; Sun, L. T.; Banhart, F. *Nat. Nanotechnol.* **2007**, *2*, 307−311.
(108) Saadi, S.; Abild-Pedersen, F.; Helveg, S.; Sehested, J.; Hinnemann, B.; Appel, C. C.; Norskov, J. K. *J. Phys. Chem. C* **2010**, *114*, 11221−11227.
(109) Hofmann, S.; Csanyi, G.; Ferrari, A. C.; Payne, M. C.; Robertson, J. *Phys. Rev. Lett.* **2005**, *95*, 036101.
(110) Kang, B. J.; Mun, J. H.; Hwang, C. Y.; Cho, B. J. *J. Appl. Phys.* **2009**, *106*, 104309.
(111) Peng, Z.; Somodi, F.; Helveg, S.; Kisielowski, C.; Specht, P.; Bell, A. T. *J. Catal.* **2012**, *286*, 22−29.
(112) Duprez, D.; Demicheli, M. C.; Marecot, P.; Barbier, J.; Ferretti, O. A.; Ponzi, E. N. *J. Catal.* **1990**, *124*, 324−335.
(113) Soykal, I. I.; Sohn, H.; Ozkan, U. S. *ACS Catal.* **2012**, *2*, 2335−2348.
(114) Mu, R.; Guo, X.; Fu, Q.; Bao, X. *J. Phys. Chem. C* **2011**, *115*, 20590−20595.
(115) Skoplyak, O.; Barteau, M. A.; Chen, J. G. *J. Phys. Chem. B* **2006**, *110*, 1686−1694.
(116) Sanchez-Sanchez, M. C.; Navarro Yerga, R. M.; Kondarides, D. I.; Verykios, X. E.; Fierro, J. L. G. *J. Phys. Chem. A* **2009**, *114*, 3873−3882.
(117) Campbell, C. T. *Annu. Rev. Phys. Chem.* **1990**, *41*, 775−837.
(118) Guo, W.; Stamatakis, M.; Vlachos, D. G. *ACS Catal.* **2013**, *3*, 2248−2255.
(119) Zafeiratos, S.; Piccinin, S.; Teschner, D. *Catal. Sci. Technol.* **2012**, *2*, 1787−1801.
(120) Yu, W.; Porosoff, M. D.; Chen, J. G. *Chem. Rev.* **2012**, *112*, 5780−5817.
(121) Alonso, D. M.; Wettstein, S. G.; Dumesic, J. A. *Chem. Soc. Rev.* **2012**, *41*, 8075−8098.
(122) Sankar, M.; Dimitratos, N.; Miedziak, P. J.; Wells, P. P.; Kiely, C. J.; Hutchings, G. J. *Chem. Soc. Rev.* **2012**, *41*, 8099−8139.
(123) Jacobsen, C. J. H.; Dahl, S. r.; Clausen, B. S.; Bahn, S.; Logadottir, A.; Norskov, J. K. *J. Am. Chem. Soc.* **2001**, *123*, 8404−8405.
(124) Wei, Z. H.; Sun, J. M.; Li, Y.; Datye, A. K.; Wang, Y. *Chem. Soc. Rev.* **2012**, *41*, 7994−8008.
(125) Larsen, J. H.; Chorkendorff, I. *Surf. Sci. Rep.* **1999**, *35*, 165−222.
(126) Parizotto, N. V.; Rocha, K. O.; Damyanova, S.; Passos, F. B.; Zanchet, D.; Marques, C. M. P.; Bueno, J. M. C. *Appl. Catal., A* **2007**, *330*, 12−22.
(127) Skoplyak, O.; Menning, C. A.; Barteau, M. A.; Chen, J. G. *Top. Catal.* **2008**, *51*, 49−59.
(128) Skoplyak, O.; Barteau, M. A.; Chen, J. G. *Catal. Today* **2009**, *147*, 150−157.
(129) Avila-Neto, C. N. Sobre a estabilidade de catalisadores de cobalto suportados durante a reforma do etanol. Ph.D. Thesis, Universidade Federal de São Carlos, June 2012.
(130) Ávila-Neto, C. N.; Zanchet, D.; Hori, C. E.; Ribeiro, R. U.; Bueno, J. M. C. *J. Catal.* **2013**, *307*, 222−237.
(131) Calvin, S.; Luo, S. X.; Caragianis-Broadbridge, C.; McGuinness, J. K.; Anderson, E.; Lehman, A.; Wee, K. H.; Morrison, S. A.; Kurihara, L. K. *Appl. Phys. Lett.* **2005**, *87*, 233102.
(132) Marino, F. J.; Cerrella, E. G.; Duhalde, S.; Jobbagy, M.; Laborde, M. A. *Int. J. Hydrogen Energy* **1998**, *23*, 1095−1101.
(133) Calles, J. A.; Carrero, A.; Vizcaino, A. J. *Microporous Mesoporous Mater.* **2009**, *119*, 200−207.
(134) Carrero, A.; Calles, J. A.; Vizcaino, A. J. *Appl. Catal., A* **2007**, *327*, 82−94.
(135) Carrero, A.; Calles, J. A.; Vizcaino, A. J. *Chem. Eng. J.* **2010**, *163*, 395−402.
(136) Chen, L.-C.; Lin, S. D. *Appl. Catal., B* **2011**, *106*, 639−649.
(137) Marino, F.; Baronetti, G.; Jobbagy, M.; Laborde, M. *Appl. Catal., A* **2003**, *238*, 41−54.
(138) Biswas, P.; Kunzru, D. *Catal. Lett.* **2007**, *118*, 36−49.
(139) Wang, F.; Li, Y.; Cai, W.; Zhan, E.; Mu, X.; Shen, W. *Catal. Today* **2009**, *146*, 31−36.
(140) Velu, S.; Suzuki, K.; Vijayaraj, M.; Barman, S.; Gopinath, C. S. *Appl. Catal., B* **2005**, *55*, 287−299.
(141) Casanovas, A.; Llorca, J.; Homs, N.; Fierro, J. L. G.; Ramirez de la Piscina, P. *J. Mol. Catal. A: Chem.* **2006**, *250*, 44−49.
(142) Jeroro, E.; Vohs, J. M. *J. Phys. Chem. C* **2009**, *113*, 1486−1494.
(143) Borgna, A.; Anderson, B. G.; Saib, A. M.; Bluhm, H.; Havecker, M.; Knop-Gericke, A.; Kuiper, A. E. T.; Tamminga, Y.; Niemantsverdriet, J. W. *J. Phys. Chem. B* **2004**, *108*, 17905−17914.
(144) Papaefthimiou, V.; Dintzer, T.; Dupuis, V.; Tamion, A.; Tournus, F.; Teschner, D.; Havecker, M.; Knop-Gericke, A.; Schlogl, R.; Zafeiratos, S. *J. Phys. Chem. Lett.* **2011**, *2*, 900−904.
(145) Braga, A. H., Catalisadores bimetálicos de Co e Ni aplicados à reforma à vapor do etanol: propriedades de oxiredução na resistência à deposição de carbono. M.S. Thesis. Universidade Federal de São Carlos, March 2012.
(146) Andonova, S.; de Avila, C. N.; Arishtirova, K.; Bueno, J. M. C.; Damyanova, S. *Appl. Catal., B* **2011**, *105*, 346−360.
(147) Resini, C.; Delgado, M. C. H.; Presto, S.; Alemany, L. J.; Riani, P.; Marazza, R.; Ramis, G.; Busca, G. *Int. J. Hydrogen Energy* **2008**, *33*, 3728−3735.

DOI: 10.1021/cs5020755
ACS Catal. 2015, 5, 3841−3863

(148) Chen, L.; Choong, C. K. S.; Zhong, Z.; Huang, L.; Wang, Z.; Lin, J. *Int. J. Hydrogen Energy* **2012**, *37*, 16321−16332.
(149) Yee, A.; Morrison, S. J.; Idriss, H. *J. Catal.* **1999**, *186*, 279−295.
(150) Vayssilov, G. N.; Mihaylov, M.; Petkov, P. S.; Hadjiivanov, K. I.; Neyman, K. M. *J. Phys. Chem. C* **2011**, *115*, 23435−23454.
(151) Mullins, D. R. *Surf. Sci. Rep.* **2015**, *70*, 42−85.
(152) He, Z.; Wang, X. *Catal. Today* **2015**, *240* (Part B), 220−228.
(153) Vohs, J. M. *Chem. Rev.* **2013**, *113*, 4136−4163.
(154) de Lima, S. M.; da Cruz, I. O.; Jacobs, G.; Davis, B. H.; Mattos, L. V.; Noronha, F. B. *J. Catal.* **2008**, *257*, 356−368.
(155) de Lima, S. M.; Silva, A. M.; Graham, U. M.; Jacobs, G.; Davis, B. H.; Mattos, L. V.; Noronha, F. B. *Appl. Catal., A* **2009**, *352*, 95−113.
(156) Mullins, D. R.; Senanayake, S. D.; Chen, T. L. *J. Phys. Chem. C* **2010**, *114*, 17112−17119.
(157) Chen, H.-L.; Liu, S.-H.; Ho, J.-J. *J. Phys. Chem. B* **2006**, *110*, 14816−14823.
(158) Li, M.; Wu, Z.; Overbury, S. H. *J. Catal.* **2013**, *306*, 164−176.
(159) Mann, A. K. P.; Wu, Z.; Calaza, F. C.; Overbury, S. H. *ACS Catal.* **2014**, *4*, 2437−2448.
(160) Chen, T. L.; Mullins, D. R. *J. Phys. Chem. C* **2011**, *115*, 3385−3392.
(161) Mullins, D. R.; Albrecht, P. M. *J. Phys. Chem. C* **2013**, *117*, 14692−14700.
(162) Wu, Z.; Li, M.; Overbury, S. H. *J. Catal.* **2012**, *285*, 61−73.
(163) Mullins, D. R.; Albrecht, P. M.; Chen, T.-L.; Calaza, F. C.; Biegalski, M. D.; Christen, H. M.; Overbury, S. H. *J. Phys. Chem. C* **2012**, *116*, 19419−19428.
(164) Lykhach, Y.; Johánek, V.; Aleksandrov, H. A.; Kozlov, S. M.; Happel, M.; Skala, T.; Petkov, P. S.; Tsud, N.; Vayssilov, G. N.; Prince, K. C.; Neyman, K. M.; Matolin, V.; Libuda, J. *J. Phys. Chem. C* **2012**, *116*, 12103−12113.
(165) Agarwal, S.; Lefferts, L.; Mojet, B. L. *ChemCatChem* **2013**, *5*, 479−489.
(166) Mullins, D.; Albrecht, P.; Calaza, F. *Top. Catal.* **2013**, *56*, 1345−1362.
(167) Soykal, I. I.; Bayram, B.; Sohn, H.; Gawade, P.; Miller, J. T.; Ozkan, U. S. *Appl. Catal., A* **2012**, *449*, 47−58.
(168) Soykal, I. I.; Sohn, H.; Singh, D.; Miller, J. T.; Ozkan, U. S. *ACS Catal.* **2014**, *4*, 585−592.
(169) Greenler, R. G. *J. Chem. Phys.* **1962**, *37*, 2094−2100.
(170) Lamotte, J.; Saur, O.; Lavalley, J. C.; Busca, G.; Rossi, P. F.; Lorenzelli, V. *J. Chem. Soc., Faraday Trans. 1* **1986**, *82*, 3019−3023.
(171) DeWilde, J. F.; Czopinski, C. J.; Bhan, A. *ACS Catal.* **2014**, *4*, 4425−4433.
(172) Christiansen, M. A.; Mpourmpakis, G.; Vlachos, D. G. *J. Catal.* **2015**, *323*, 121−131.
(173) Roy, S.; Mpourmpakis, G.; Hong, D.-Y.; Vlachos, D. G.; Bhan, A.; Gorte, R. J. *ACS Catal.* **2012**, *2*, 1846−1853.
(174) Jenness, G. R.; Christiansen, M. A.; Caratzoulas, S.; Vlachos, D. G.; Gorte, R. J. *J. Phys. Chem. C* **2014**, *118*, 12899−12907.
(175) Akhter, S.; Cheng, W. H.; Lui, K.; Kung, H. H. *J. Catal.* **1984**, *85*, 437−456.
(176) Chung, J. S.; Miranda, R.; Bennett, C. O. *J. Chem. Soc., Faraday Trans. 1* **1985**, *81*, 19−36.
(177) Abe, H.; Maruya, K.; Domen, K.; Onishi, T. *Chem. Lett.* **1984**, 1875−1878.
(178) Spitz, R. N.; Barton, J. E.; Barteau, M. A.; Staley, R. H.; Sleight, A. W. *J. Phys. Chem.* **1986**, *90*, 4067−4075.
(179) Chieregato, A.; Ochoa, J. V.; Bandinelli, C.; Fornasari, G.; Cavani, F.; Mella, M. *ChemSusChem* **2015**, *8*, 377−388.
(180) Szijjarto, G. P.; Paszti, Z.; Sajo, I.; Erdohelyi, A.; Radnoczi, G.; Tompos, A. *J. Catal.* **2013**, *305*, 290−306.
(181) Di Cosimo, J. I.; Apesteguía, C. R.; Ginés, M. J. L.; Iglesia, E. *J. Catal.* **2000**, *190*, 261−275.
(182) Idriss, H.; Seebauer, E. G. *J. Mol. Catal. A: Chem.* **2000**, *152*, 201−212.
(183) Nair, H.; Gatt, J. E.; Miller, J. T.; Baertsch, C. D. *J. Catal.* **2011**, *279*, 144−154.
(184) Zhou, G.; Barrio, L.; Agnoli, S.; Senanayake, S. D.; Evans, J.; Kubacka, A.; Estrella, M.; Hanson, J. C.; Martínez-Arias, A.; Fernández-García, M.; Rodriguez, J. A. *Angew. Chem., Int. Ed.* **2010**, *49*, 9680−9684.
(185) Cai, W.; Wang, F.; Zhan, E.; Van Veen, A. C.; Mirodatos, C.; Shen, W. *J. Catal.* **2008**, *257*, 96−107.
(186) Cai, W.; Wang, F.; Daniel, C. c.; van Veen, A. C.; Schuurman, Y.; Descorme, C.; Provendier, H. l. n.; Shen, W.; Mirodatos, C. *J. Catal.* **2012**, *286*, 137−152.
(187) Sadovskaya, E. M.; Ivanova, Y. A.; Pinaeva, L. G.; Grasso, G.; Kuznetsova, T. G.; van Veen, A.; Sadykov, V. A.; Mirodatos, C. *J. Phys. Chem. A* **2007**, *111*, 4498−4505.
(188) Pierre, D.; Deng, W.; Flytzani-Stephanopoulos, M. *Top. Catal.* **2007**, *46*, 363−373.
(189) Rodriguez, J. A.; Liu, P.; Hrbek, J.; Evans, J.; Perez, M. *Angew. Chem., Int. Ed.* **2007**, *46*, 1329−1332.
(190) Williams, W. D.; Shekhar, M.; Lee, W.-S.; Kispersky, V.; Delgass, W. N.; Ribeiro, F. H.; Kim, S. M.; Stach, E. A.; Miller, J. T.; Allard, L. F. *J. Am. Chem. Soc.* **2010**, *132*, 14018−14020.
(191) Bruix, A.; Rodriguez, J. A.; Ramirez, P. J.; Senanayake, S. D.; Evans, J.; Park, J. B.; Stacchiola, D.; Liu, P.; Hrbek, J.; Illas, F. *J. Am. Chem. Soc.* **2012**, *134*, 8968−8974.
(192) Aranifard, S.; Ammal, S. C.; Heyden, A. *J. Catal.* **2014**, *309*, 314−324.
(193) He, Z.; Yang, M.; Wang, X.; Zhao, Z.; Duan, A. *Catal. Today* **2012**, *194*, 2−8.
(194) Song, H.; Ozkan, U. S. *J. Catal.* **2009**, *261*, 66−74.
(195) Martono, E.; Vohs, J. M. *J. Catal.* **2012**, *291*, 79−86.
(196) Martono, E.; Hyman, M. P.; Vohs, J. M. *Phys. Chem. Chem. Phys.* **2011**, *13*, 9880−9886.
(197) Song, H.; Bao, X.; Hadad, C.; Ozkan, U. *Catal. Lett.* **2011**, *141*, 43−54.
(198) Volanti, D. P.; Sato, A. G.; Orlandi, M. O.; Bueno, J. M. C.; Longo, E.; Andres, J. *ChemCatChem* **2011**, *3*, 839−843.
(199) Sato, A. G.; Volanti, D. P.; de Freitas, I. C.; Longo, E.; Bueno, J. M. C. *Catal. Commun.* **2012**, *26*, 122−126.
(200) Sato, A. G.; Volanti, D. P.; Meira, D. M.; Damyanova, S.; Longo, E.; Bueno, J. M. C. *J. Catal.* **2013**, *307*, 1−17.
(201) Xu, W.; Liu, Z.; Johnston-Peck, A. C.; Senanayake, S. D.; Zhou, G.; Stacchiola, D.; Stach, E. A.; Rodriguez, J. A. *ACS Catal.* **2013**, *3*, 975−984.
(202) Galetti, A. E.; Gomez, M. F.; Arrua, L. A.; Cristina Abello, M. *Appl. Catal., A* **2008**, *348*, 94−102.
(203) Nagai, Y.; Dohmae, K.; Ikeda, Y.; Takagi, N.; Tanabe, T.; Hara, N.; Guilera, G.; Pascarelli, S.; Newton, M. A.; Kuno, O.; Jiang, H.; Shinjoh, H.; Matsumoto, S. i. *Angew. Chem., Int. Ed.* **2008**, *47*, 9303−9306.
(204) Kaddouri, A.; Mazzocchia, C. *Catal. Commun.* **2004**, *5*, 339−345.
(205) Li, S.; Li, M.; Zhang, C.; Wang, S.; Ma, X.; Gong, J. *Int. J. Hydrogen Energy* **2012**, *37*, 2940−2949.
(206) da Silva, A. M.; de Souza, K. R.; Mattos, L. V.; Jacobs, G.; Davis, B. H.; Noronha, F. B. *Catal. Today* **2011**, *164*, 234−239.
(207) Laosiripojana, N.; Assabumrungrat, S.; Charojrochkul, S. *Appl. Catal., A* **2007**, *327*, 180−188.
(208) Coleman, L. J. I.; Epling, W.; Hudgins, R. R.; Croiset, E. *Appl. Catal., A* **2009**, *363*, 52−63.
(209) Sanchez-Sanchez, M. C.; Navarro, R. M.; Fierro, J. L. G. *Int. J. Hydrogen Energy* **2007**, *32*, 1462−1471.
(210) Di Cosimo, J. I.; Diez, V. K.; Xu, M.; Iglesia, E.; Apesteguia, C. R. *J. Catal.* **1998**, *178*, 499−510.
(211) Zotov, R. A.; Molchanov, V. V.; Volodin, A. M.; Bedilo, A. F. *J. Catal.* **2011**, *278*, 71−77.
(212) Chiang, H.; Bhan, A. *J. Catal.* **2010**, *271*, 251−261.
(213) Birky, T. W.; Kozlowski, J. T.; Davis, R. J. *J. Catal.* **2013**, *298*, 130−137.
(214) Nadeem, A. M.; Waterhouse, G. I. N.; Idriss, H. *Catal. Today* **2012**, *182*, 16−24.

DOI: 10.1021/cs5020755
ACS Catal. 2015, 5, 3841−3863

(215) Rekoske, J. E.; Barteau, M. A. *Ind. Eng. Chem. Res.* **2011**, *50*, 41−51.
(216) Nishiguchi, T.; Matsumoto, T.; Kanai, H.; Utani, K.; Matsumura, Y.; Shen, W. J.; Imamura, S. *Appl. Catal., A* **2005**, *279*, 273−277.
(217) Idriss, H.; Diagne, C.; Hindermann, J. P.; Kiennemann, A.; Barteau, M. A. *J. Catal.* **1995**, *155*, 219−237.
(218) Kiennemann, A.; Idriss, H.; Kieffer, R.; Chaumette, P.; Durand, D. *Ind. Eng. Chem. Res.* **1991**, *30*, 1130−1138.
(219) Nakajima, T.; Nameta, H.; Mishima, S.; Matsuzaki, I.; Tanabe, K. *J. Mater. Chem.* **1994**, *4*, 853−858.
(220) Sun, J.; Karim, A. M.; Mei, D.; Engelhard, M.; Bao, X.; Wang, Y. *Appl. Catal., B* **2015**, *162*, 141−148.
(221) Youn, M. H.; Seo, J. G.; Lee, H.; Bang, Y.; Chung, J. S.; Song, I. K. *Appl. Catal., B* **2010**, *98*, 57−64.
(222) Frusteri, F.; Freni, S.; Chiodo, V.; Spadaro, L.; Bonura, G.; Cavallaro, S. *J. Power Sources* **2004**, *132*, 139−144.
(223) Frusteri, F.; Freni, S.; Chiodo, V.; Spadaro, L.; Di Blasi, O.; Bonura, G.; Cavallaro, S. *Appl. Catal., A* **2004**, *270*, 1−7.
(224) Llorca, J.; Homs, N.; Sales, J.; Fierro, J. L. G.; de la Piscina, P. R. *J. Catal.* **2004**, *222*, 470−480.
(225) Domok, M.; Baan, K.; Kecskes, T.; Erdohelyi, A. *Catal. Lett.* **2008**, *126*, 49−57.
(226) Roh, H.-S.; Platon, A.; Wang, Y.; King, D. L. *Catal. Lett.* **2006**, *110*, 1−6.
(227) Choong, C. K. S.; Huang, L.; Zhong, Z.; Lin, J.; Hong, L.; Chen, L. *Appl. Catal., A* **2011**, *407*, 155−162.
(228) Song, H.; Ozkan, U. S. *J. Phys. Chem. A* **2010**, *114*, 3796−3801.
(229) Granados, M. L.; Gurbani, A.; Mariscal, R.; Fierro, J. L. G. *J. Catal.* **2008**, *256*, 172−182.

DOI: 10.1021/cs5020755
ACS Catal. 2015, 5, 3841−3863